

# Detection of X-ray emission from the host clusters of 3CR quasars

C. S. Crawford,<sup>1</sup> I. Lehmann,<sup>2</sup> A. C. Fabian,<sup>1</sup> M. N. Bremer<sup>3</sup> and G. Hasinger<sup>2</sup>

<sup>1</sup>*Institute of Astronomy, Madingley Road, Cambridge CB3 0HA*

<sup>2</sup>*Astrophysikalisches Institut Potsdam, An der Sternwarte 16, D-14482 Potsdam, Germany*

<sup>3</sup>*Department of Physics, University of Bristol, Tyndall Avenue, Bristol BS8 1TL*

Accepted 1999 May 11. Received 1999 April 28; in original form 1999 January 25

## ABSTRACT

We report the detection of extended X-ray emission around several powerful 3CR quasars with redshifts out to 0.73. The *ROSAT* HRI images of the quasars have been corrected for spacecraft wobble and compared with an empirical point-spread function. All the quasars examined show excess emission at radii of 15 arcsec and more, the evidence being strong for the more distant objects and weak only for the two nearest ones, which are known from other wavelengths not to lie in strongly clustered environments. The spatial profile of the extended component is consistent with thermal emission from the intracluster medium of moderately rich host clusters to the quasars. The total luminosities of the clusters are in the range  $\sim 4 \times 10^{44} - 3 \times 10^{45} \text{ erg s}^{-1}$ , assuming a temperature of 4 keV. The inner regions of the intracluster medium are, in all cases, dense enough to be part of a cooling flow.

**Key words:** galaxies: clusters: general – cooling flows – quasars: general – X-rays: galaxies.

## 1 INTRODUCTION

The two most powerful FR II radio sources in the nearby Universe – Cyg A and 3C295 – are each located at the centre of a dense, moderately rich cluster of galaxies. While such an environment is exceptional for a low-redshift FR II galaxy, it appears to be common around powerful radio objects at earlier epochs. Above a redshift of 0.5, radio-loud objects (both the quasars and radio galaxies) are inferred to lie in clusters of galaxies of moderate optical richness. The evidence for such an environment includes optical and near-IR galaxy counts (Yee & Green 1987; Yates, Miller & Peacock 1989; Hill & Lilly 1991; Ellingson, Yee & Green 1991; Dickinson 1997), high gas pressures within a radius of 30 kpc (Crawford & Fabian 1989; Forbes et al. 1990; Bremer et al. 1992; Durret et al. 1994), cD-type host galaxy profiles (Best, Longair & Rottgering 1998), a gravitational arc (Deltorn et al. 1997) and lensing shear of surrounding field galaxies (Bower & Smail 1997). The properties of the radio source itself also imply the presence of a confining medium: a large-scale working surface on which the jets form the radio lobes, a steep radio spectrum and a high minimum pressure in regions of relaxed radio structure (Bremer et al. 1992). A Faraday depolarization asymmetry (Garrington & Conway 1991), the distortion and compression of high-redshift radio source morphologies (Hintzen, Ulvestad & Owen 1983; Barthel & Miley 1988) and sources with very high Faraday rotation measures (Carilli, Owen & Harris 1994; Carilli et al. 1997) all corroborate the inference of a dense, clumpy medium surrounding the radio source. Thus it appears that the deepest

potential wells we can readily pinpoint at  $z \geq 1$  are those around powerful radio sources.

The cluster distribution at high redshift can provide a stringent cosmological test (see e.g. Donahue et al. 1998), and can also be compared with the X-ray luminosity function of clusters at low redshift (e.g. Ebeling et al. 1997). Whilst it may result in a sample of clusters biased to only those that can host an active nucleus, using radio sources to identify the location of deep potential wells is a promising way of finding clusters out to and beyond a redshift  $z \sim 1$  (Crawford 1997). Current X-ray surveys of clusters detected from the *ROSAT* All-Sky Survey (e.g. Ebeling et al. 1998) do not reach sufficiently faint flux levels, and studies of deep serendipitous X-ray pointings (e.g. Rosati et al. 1998) cover only a small fraction of the sky. The first step, however, is simply to confirm that powerful radio quasars beyond a redshift of a half really do lie at the centres of clusters of galaxies.

The clearest way to determine directly the presence of a cluster of galaxies is to detect thermal X-ray emission from its hot intracluster medium. A certain degree of success has been achieved in detecting and spatially resolving the X-ray emission around distant ( $0.5 < z < 2$ ) radio galaxies using *ROSAT* (Crawford & Fabian 1993; Worrall et al. 1994; Crawford & Fabian 1995a, 1996a,b; Crawford 1997; Dickinson 1997; Hardcastle, Lawrence & Worrall 1998; Carilli et al. 1998). Any X-rays emitted by the central bright nucleus of radio galaxies are assumed to be absorbed along the line of sight, as observed for the powerful low-redshift radio galaxy Cygnus A (Ueno et al. 1994). The inferred bolometric luminosity of the X-ray sources associated

with the radio galaxies is  $\sim 0.7\text{--}18 \times 10^{44} \text{ erg s}^{-1}$ , easily compatible with that expected from moderately rich clusters of galaxies around the radio sources. There could also be a contribution to the extended X-ray emission from inverse Compton scattering of the hidden quasar radiation (e.g. Brunetti, Setti & Comastri 1997).

In the case of radio quasars, however, the X-ray detection of the spatially extended environment is complicated by the presence of bright spatially unresolved X-ray emission from the active nucleus. The *ROSAT* PSPC did not combine the necessary sensitivity with a sufficiently good point-response function, needed to both detect and resolve any cluster emission around quasars. Upper limits of  $1.6\text{--}3.5 \times 10^{44} \text{ erg s}^{-1}$  (in the 0.1–2.4 keV rest-frame band) to X-ray emission from the environment of three radio-loud quasars have been derived from *ROSAT* HRI data (Hall et al. 1995; Hall, Ellingson & Green 1997), assuming the cluster emission profile is modelled by a King law.

We have also obtained *ROSAT* HRI data to resolve and detect spatially the extended emission from the intracluster medium around each of a small sample of intermediate-redshift radio-loud quasars. The detection of such a component is, however, complicated by the wobble of the spacecraft during the observation. This occurs on a  $\sim 402\text{-s}$  period, and, when the attitude of the spacecraft is not well reconstructed, leads to smearing of the point-spread function (PSF). The bright emission from the quasar nucleus can then contaminate the outer regions where we hope to detect emission from any surrounding cluster, and this has so far hindered our progress in interpreting the data. In this paper, however, we present an analysis of our *ROSAT* HRI data taken for seven intermediate-redshift ( $0.1 < z < 0.8$ ) radio-loud quasars, which employs a new correction for the spacecraft wobble derived by Harris et al. (1998).

A contemporaneous and independent analysis of an overlapping data set using this technique has been carried out by Hardcastle & Worrall (1999), who obtain similar results.

## 2 OBSERVATIONS AND ANALYSIS

We use the *ROSAT* data of intermediate-redshift, radio-loud

quasars for which there is prior evidence from other wavebands for a cluster environment (see notes on individual quasars for details). We preferentially selected quasars of only moderate X-ray luminosity in order to minimize the contrast between the nuclear emission and any cluster emission. These targets were supplemented by data available from the *ROSAT* public archive on 3C273 and 3C215. We also include the observations of H1821+643 to form a comparison with the results of Hall et al. (1997). The observations used, and details of the quasars, are listed in Table 1.

### 2.1 Wobble-correction technique

The spatial analysis of *ROSAT* HRI observations is often complicated by smearing of the image, of the order of 10 arcsec (Morse 1994). This degradation of the intrinsic resolution of the HRI instrument (5 arcsec) can be induced by errors in the aspect solution associated with the wobble of the *ROSAT* spacecraft, or with the reacquisition of the guide stars. To counteract this effect, we use the wobble-correction technique of Harris et al. (1998), which minimizes the spatial smearing of the sources. The technique is based on the simple assumption that in the case of a stable roll angle (i.e. the same guide star configuration) the aspect error is repeated through each cycle of the wobble. We thus selected data only from the longest constant roll angle interval of an observation and folded these data over the *ROSAT* 402-s wobble phase. This phase was grouped into a number of intervals (5, 10 or 20) in order to calculate phase-resolved subimages. The centroid of each of the subimages was calculated by fitting a two-dimensional Gaussian to the brightest source near the field centre. The wobble-corrected HRI events list is reconstructed by adding the subimages, which have been shifted to the centroid position of the uncorrected HRI image. If a subimage contains too few photons with which to determine the centroid, then the position of the subimage is not changed. This makes sure that source extension cannot be produced by a failure of the centroid determination in one or more subimages.

For X-ray sources with count rates  $\sim 0.1 \text{ count s}^{-1}$  the method

**Table 1.** Target sample and results.

| Quasar    | RA<br>(J2000) | Dec.<br>(J2000) | Redshift<br>$z$ | $N_{\text{H}}$<br>( $10^{20} \text{ cm}^{-2}$ ) | ROR       | Exposure<br>(sec) | Roll angle<br>interval |
|-----------|---------------|-----------------|-----------------|---|-----------|-------------------|------------------------|
| 3C48      | 01 37 41.3    | 33 09 35        | 0.367           | 4.54  | 800634n00 | 37362             | 1-60000                |
| 3C215     | 09 06 31.9    | 16 46 13        | 0.412           | 3.65  | 800753a01 | 39173             | 27000-58000            |
|           |               |                 |                 |   | 800753n00 | 17231             | 14000-22000            |
|           |               |                 |                 |   | 800718n00 | 16148             | 1-50000                |
| 3C254     | 11 14 38.5    | 40 37 20        | 0.734           | 1.90  | 800721n00 | 29162             | 29000-49000            |
| 3C273     | 12 29 06.7    | 02 03 09        | 0.158           | 1.79  | 701576n00 | 68154             | 1-32000                |
| 3C275.1   | 12 43 57.7    | 16 22 53        | 0.555           | 1.99  | 800719n00 | 25396             | 9000-32000             |
| 3C281     | 13 07 53.9    | 06 42 13        | 0.602           | 2.21  | 800635a01 | 20299             | 12000-24000            |
|           |               |                 |                 |   | 800635n00 | 18220             | 1-14000                |
| 3C334     | 16 20 21.5    | 17 36 29        | 0.555           | 4.24  | 800720n00 | 28183             | 17000-42000            |
| H1821+643 | 18 21 57.3    | 64 20 36        | 0.297           | 4.04  | 800754n00 | 29427             | 23000-31000            |

Notes:

Further possible observations of 3C215 (800718a01), 3C194 (800803n00) and 3C280 (800802n00) all had too few photons in the source for a satisfactory wobble correction.

The hydrogen column density along the line of sight to each quasar ( $N_{\text{H}}$ ) is calculated from the data of Stark et al. (1992).

ROR in column 6 is the *ROSAT* observation request sequence number.

The roll angle interval tabulated in the final column is given in sequence numbers taken from the attitude file, which contains the attitude information of the telescope (such that roll angle x1 at time y1 gives sequence number 1). The time interval of the spacecraft clock is 1 s. Sequence numbers from 1 to 34000 thus mean that the data is extracted from between the time y1 and the time y34000 (34000 s).

can reduce the full width at half maximum by about 30 per cent (cf. Harris et al. 1998). The efficacy of this technique has been tested on HRI observations of low-luminosity X-ray active galactic nuclei (AGN), some of which show no sign of extended X-ray emission once corrected for wobble (Lehmann et al. 1999). We cannot apply the wobble-correction technique to all possible data for suitable targets in the literature, as it can only be applied to observations that have a sufficient number of photons within a constant spacecraft roll angle (cf. Table 1).

## 2.2 Radial profile analysis

Our aim is to search for spatially extended X-ray emission originating in any intracluster medium around the quasars. We have derived a background-subtracted radial profile from the uncorrected and wobble-corrected HRI data of the X-ray source associated with each quasar. First we determined the centroid position of the X-ray source by fitting a two-dimensional Gaussian. Then we calculated the counts per arcsec<sup>2</sup> within the rings around the centroid position from 0–2.5 arcsec in steps of 0.5 arcsec, from 2.5–15 arcsec in steps of 2.5 arcsec, from 15–100 arcsec in steps of 12.5 arcsec and from 100–1000 arcsec in steps of 100 arcsec. The background value was calculated as the median from the six rings between 300 and 900 arcsec. Finally we subtracted the background value from each ring.

First, however, we need to model the HRI PSF accurately, which will allow us to remove the contaminating spill-over of light from the bright quasar nucleus. The standard HRI PSF of David et al. (1995) does not provide a good fit to the radial profile of observed point sources (see Fig. 1). This deviation is particularly acute where the PSF shows a sharp drop at radii between 10 and 30 arcsec, where we expect the contrast between the nuclear source and any extended cluster emission to begin to show. Instead we have determined a good analytical characterization to an empirical PSF derived from observations of 21 *ROSAT* Bright Survey stars, each of which has undergone the same wobble correction procedure as the quasar data. Our best fit is the sum of two Gaussians and a power-law component (Fig. 1). Assuming that this PSF forms a good model for the spillover of

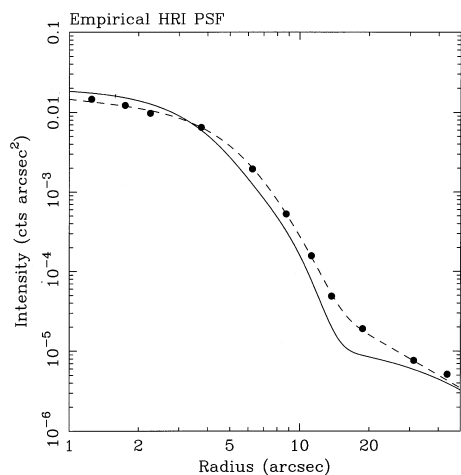


**Figure 1.** The best-fitting analytic model (dashed line) to the empirically derived HRI PSF (circle markers), shown with an arbitrary flux scaling. The solid line shows the standard HRI PSF of David et al. (1995) for comparison.

quasar nuclear light, we fix the relative normalizations and widths of the three components and leave the overall normalization  $n$  of this profile as the only free variable in the function:

$$I(r) = n\{e^{-0.5(r/4.5001)^2} + 4.376e^{-0.5(r/2.8644)^2} + 0.9346r^{-1.6569}\}.$$

We follow the same procedure for the profile fitting of each quasar. First we fit the profile by the empirically derived HRI PSF alone, allowing its normalization to vary freely. We then fit this PSF (with normalization still free to vary) in combination with each of two models chosen to represent any extended emission. The first model is a broken power law, with slope  $r^{-1}$  for radii  $r < R$  and  $r^{-2.1}$  for  $r \geq R$ , where the break  $R$  and the absolute normalization of the extended component are free to vary. This is an approximation to the X-ray surface brightness profile of the gas in a typical cluster of galaxies containing a cooling flow, and  $R$  then corresponds to the cooling radius (e.g. Crawford & Fabian 1995b). The second model employed is a projected King law, with index fixed at  $-1.5$ , and the core radius  $R$  and normalization left as free parameters. Given the errors inherent in these model, and the question of whether such simple models truly characterize the extended emission, we do not convolve the extended emission models with the PSF. The relative normalization between the PSF and extended components is not always very well determined, so we also derive what should be regarded as a lower limit to the presence of any extended component by assuming that the nuclear emission accounts for all the light in the X-ray core. We fit the PSF to the quasar radial profile within the inner 1–5 arcsec and then subtract this model and fit the residuals by each of the cluster models. We execute these five model fits to the profiles out to a radius of 50 arcsec (11 data points), yielding 10, 8 and 9 degrees of freedom for the PSF only, PSF + extended component models, and the fit of the extended component model to the residual after subtraction of the normalized HRI PSF. We then repeat the fits to the profile out to a radius of 100 arcsec (15 data points), yielding 14, 12 and 13 degrees of freedom to the fits as above. The fitting analysis is carried out first for each quasar image in the absence of any wobble correction, and then for the images corrected using different phase intervals.

The detailed results are summarized in Table 2, where the reduced  $\chi^2$  is given for each fit. We tabulate the best-fitting parameters of the profile fits out to a radius of 50 arcsec and then 100 arcsec in turn:  $R$  (in arcsec) representing either the break in the broken power-law model, or the core radius in the King law model; the integrated luminosity of the extended component as a percentage of the total luminosity of the X-ray source; the X-ray luminosities (in the observed 0.1–2 keV energy band) of the quasar component ( $L_X^{\text{QSO}}$ ) and the cluster component ( $L_X^{\text{cl}}$ ) assuming a power-law of photon index 2 and thermal bremsstrahlung emission at a temperature of  $kT = 4$  keV respectively. (At the redshift of our quasars this observed band carries about half of the bolometric luminosity for the thermal spectrum.) The errors are derived from propagating the  $\Delta\chi^2 = 1$  confidence limits of the fit parameters. Errors are not shown when the fit was insufficiently robust to extract errors for all parameters of interest. Table 2, however, demonstrates the full range of values obtained from the 10 model fits employed for each of the phase intervals and allows one to assess the variation of each parameter from the systematic uncertainties of PSF normalization and the extended component model employed. A comparison of some of the better fits with the radial profile of each quasar (those shown in bold font in Table 2) is displayed in Fig. 2. These plots clearly show that

**Table 2.** Profile fitting results.

| Quasar            | phase interval<br>of correction | model<br>outer radius (arcsec) | reduced- $\chi^2$<br>(50) | $R$<br>(50)         | %<br>(50)   | $L_X^{\text{QSO}}$<br>(50) | $L_X^{\text{cl}}$<br>(50) | reduced- $\chi^2$<br>(100) | $R$<br>(100)         | %<br>(100)  | $L_X^{\text{QSO}}$<br>(100) | $L_X^{\text{cl}}$<br>(100) |
|-------------------|---------------------------------|--------------------------------|---------------------------|---------------------|-------------|----------------------------|---------------------------|----------------------------|----------------------|-------------|-----------------------------|----------------------------|
| 3C48              | no correction                   | psf                            | 36.12                     | —                   | —           | —                          | —                         | 25.84                      | —                    | —           | —                           | —                          |
|                   |                                 | psf + bpow                     | 26.86                     | $7.7^{+1.3}_{-1.5}$ | $13 \pm 4$  | 557.2                      | $63.8 \pm 20.1$           | 19.00                      | $6.6^{+2.3}_{-0.5}$  | $14 \pm 4$  | 577.2                       | $74.6 \pm 22.1$            |
|                   |                                 | psf + king                     | 20.22                     | $5.2^{+0.5}_{-0.4}$ | 20          | 510.6                      | 98.4                      | 13.57                      | $5.2^{+0.5}_{-0.4}$  | 20          | 530.6                       | 104.5                      |
|                   |                                 | bpow remainder                 | 24.20                     | $6.2^{+0.4}_{-0.2}$ | $15 \pm 1$  | 532.0                      | $74.1 \pm 6.2$            | 17.85                      | $6.3^{+0.4}_{-0.2}$  | $16 \pm 1$  | 554.4                       | $84.2 \pm 6.8$             |
|                   |                                 | king remainder                 | 18.18                     | $5.6^{+0.4}_{-0.3}$ | $17 \pm 3$  | 532.0                      | 86.5                      | 12.69                      | $5.5^{+0.5}_{-0.3}$  | $17 \pm 4$  | 554.4                       | 91.6                       |
| 3C48              | 5                               | psf                            | 16.24                     | —                   | —           | —                          | —                         | 11.65                      | —                    | —           | —                           | —                          |
|                   |                                 | psf + bpow                     | 12.73                     | 6.3                 | 12          | 590.0                      | 60.8                      | 8.87                       | $6.3^{+2.8}_{-0.3}$  | 12          | 617.1                       | 66.3                       |
|                   |                                 | psf + king                     | 9.90                      | $5.3^{+0.7}_{-0.5}$ | 16          | 559.5                      | 81.8                      | 6.67                       | $5.3^{+0.7}_{-0.5}$  | 16          | 582.6                       | 86.4                       |
|                   |                                 | bpow remainder                 | 11.56                     | $6.2^{+0.6}_{-0.4}$ | $13 \pm 2$  | 569.8                      | $67.1 \pm 8.5$            | 8.41                       | $6.2^{+0.6}_{-0.5}$  | $14 \pm 2$  | 593.8                       | $76.0 \pm 10.3$            |
|                   |                                 | king remainder                 | 8.82                      | $5.5^{+0.6}_{-0.5}$ | $14 \pm 4$  | 569.8                      | 76.3                      | 6.18                       | $5.5^{+0.6}_{-0.5}$  | $15 \pm 4$  | 593.8                       | 80.8                       |
| 3C48              | 10                              | psf                            | 9.89                      | —                   | —           | —                          | —                         | 7.13                       | —                    | —           | —                           | —                          |
|                   |                                 | psf + bpow                     | 6.00                      | $6.2^{+2.9}_{-0.5}$ | 10          | 579.0                      | 53.4                      | 4.48                       | $6.2^{+2.9}_{-0.6}$  | 11          | 628.9                       | 58.0                       |
|                   |                                 | psf + king                     | 4.55                      | $5.3^{+1.1}_{-0.7}$ | 13          | 556.5                      | 67.7                      | 4.48                       | $6.3^{+2.9}_{-0.6}$  | 17          | 607.5                       | 97.3                       |
|                   |                                 | bpow remainder                 | 5.37                      | $6.2^{+1.3}_{-0.6}$ | $11 \pm 2$  | 572.6                      | $54.0 \pm 11.0$           | 4.18                       | $M6.2^{+1.2}_{-0.7}$ | $12 \pm 2$  | 596.6                       | $61.6 \pm 12.8$            |
|                   |                                 | king remainder                 | 4.11                      | $5.8^{+0.8}_{-0.7}$ | $12 \pm 5$  | 572.6                      | 58.8                      | 2.97                       | $5.8^{+0.8}_{-0.6}$  | $12 \pm 5$  | 596.6                       | 62.2                       |
| 3C48              | 20                              | <b>psf</b>                     | <b>8.34</b>               | —                   | —           | —                          | —                         | 6.04                       | —                    | —           | —                           | —                          |
|                   |                                 | <b>psf + bpow</b>              | <b>4.78</b>               | $6.3^{+3.1}_{-0.7}$ | <b>10</b>   | <b>591.6</b>               | <b>49.3</b>               | 3.70                       | 6.3                  | 10          | 619.0                       | 53.0                       |
|                   |                                 | <b>psf + king</b>              | <b>3.60</b>               | $5.3^{+1.2}_{-0.8}$ | <b>12</b>   | <b>569.5</b>               | <b>63.3</b>               | 2.56                       | $5.3^{+1.0}_{-0.9}$  | 12          | 594.2                       | 66.4                       |
|                   |                                 | bpow remainder                 | 4.28                      | $6.3^{+1.9}_{-0.7}$ | $10 \pm 3$  | 585.1                      | $50.8 \pm 13.1$           | 3.44                       | $6.3^{+1.7}_{-0.8}$  | $11 \pm 3$  | 609.7                       | $56.7 \pm 14.5$            |
|                   |                                 | king remainder                 | 3.26                      | $5.9^{+0.9}_{-0.8}$ | $11 \pm 5$  | 585.1                      | 54.5                      | 2.41                       | $5.8^{+0.9}_{-0.7}$  | $11 \pm 5$  | 609.7                       | 57.7                       |
| 3C215 (800753a01) | no correction                   | psf                            | 9.26                      | —                   | —           | —                          | —                         | 6.76                       | —                    | —           | —                           | —                          |
|                   |                                 | psf + bpow                     | 4.79                      | $6.3^{+2.9}_{-0.4}$ | $23 \pm 8$  | 145.7                      | $34.4 \pm 11.4$           | 3.29                       | $6.3^{+2.9}_{-0.4}$  | 25          | 152.1                       | 40.0                       |
|                   |                                 | psf + king                     | 3.25                      | $5.5^{+1.0}_{-0.8}$ | 27          | 135.2                      | 40.5                      | 2.29                       | $5.5^{+1.0}_{-0.8}$  | 27          | 141.6                       | 42.5                       |
|                   |                                 | bpow remainder                 | 4.27                      | $7.7^{+1.4}_{-1.6}$ | $20 \pm 6$  | 150.4                      | $30.8 \pm 9.1$            | 3.04                       | $7.6^{+1.5}_{-1.5}$  | $23 \pm 7$  | 156.7                       | $36.7 \pm 11.1$            |
|                   |                                 | king remainder                 | 3.16                      | $6.6^{+1.0}_{-0.7}$ | $20 \pm 8$  | 150.4                      | 31.1                      | 2.29                       | $6.7^{+1.0}_{-0.7}$  | $21 \pm 8$  | 156.7                       | 33.6                       |
| 3C215 (800753a01) | 5                               | psf                            | 2.94                      | —                   | —           | —                          | —                         | 2.23                       | —                    | —           | —                           | —                          |
|                   |                                 | psf + bpow                     | 1.91                      | 8.7                 | 14          | 158.3                      | 21.2                      | 1.39                       | 8.7                  | 16          | 164.9                       | 25.8                       |
|                   |                                 | psf + king                     | 1.34                      | 5.2                 | 22          | 143.1                      | 31.9                      | 1.02                       | 5.3                  | 22          | 149.5                       | 33.7                       |
|                   |                                 | bpow remainder                 | 1.71                      | $8.8^{+2.8}_{-2.7}$ | $13 \pm 6$  | 160.7                      | $19.6 \pm 8.9$            | 1.30                       | $8.7^{+2.8}_{-2.7}$  | $15 \pm 7$  | 167.4                       | $23.6 \pm 11.1$            |
|                   |                                 | king remainder                 | 1.34                      | $7.2^{+2.5}_{-1.6}$ | $14 \pm 12$ | 160.7                      | 21.4                      | 1.04                       | $7.3^{+2.5}_{-1.7}$  | $15 \pm 13$ | 167.4                       | 23.2                       |
| 3C215 (800753a01) | 10                              | psf                            | 5.25                      | —                   | —           | —                          | —                         | 3.93                       | —                    | —           | —                           | —                          |
|                   |                                 | psf + bpow                     | 3.43                      | $6.3^{+2.9}_{-0.7}$ | 23          | 141.2                      | 33.6                      | 2.49                       | $6.3^{+2.9}_{-0.7}$  | 25          | 147.5                       | 39.0                       |
|                   |                                 | psf + king                     | 2.52                      | $5.1^{+1.4}_{-1.0}$ | 30          | 125.3                      | 44.2                      | 1.86                       | $5.1^{+1.5}_{-0.9}$  | 31          | 130.0                       | 47.3                       |
|                   |                                 | bpow remainder                 | 3.05                      | $6.3^{+2.6}_{-0.6}$ | $23 \pm 7$  | 141.9                      | $33.5 \pm 10.4$           | 2.30                       | $6.2^{+2.6}_{-0.6}$  | $25 \pm 8$  | 147.9                       | $39.9 \pm 12.6$            |
|                   |                                 | king remainder                 | 2.37                      | $6.3^{+1.2}_{-0.9}$ | $23 \pm 12$ | 141.9                      | 33.6                      | 1.80                       | $6.3^{+1.2}_{-0.9}$  | $23 \pm 13$ | 147.9                       | 36.1                       |
| 3C215 (800753a01) | 15                              | <b>psf</b>                     | <b>2.94</b>               | —                   | —           | —                          | —                         | 2.23                       | —                    | —           | —                           |                            |

Table 2 – continued

| Quasar            | phase interval<br>of correction | model<br>outer radius (arcsec) | reduced- $\chi^2$<br>(50) | $R$<br>(50)            | %<br>(50) | $L_X^{\text{QSO}}$<br>(50) | $L_X^{\text{cl}}$<br>(50) | reduced- $\chi^2$<br>(100) | $R$<br>(100)          | %<br>(100) | $L_X^{\text{QSO}}$<br>(100) | $L_X^{\text{cl}}$<br>(100) |
|-------------------|---------------------------------|--------------------------------|---------------------------|------------------------|-----------|----------------------------|---------------------------|----------------------------|-----------------------|------------|-----------------------------|----------------------------|
|                   |                                 | <b>psf + bpow</b>              | <b>1.91</b>               | <b>8.7</b>             | <b>14</b> | <b>158.3</b>               | <b>21.2</b>               | 1.39                       | 8.7                   | 16         | 164.9                       | 25.8                       |
|                   |                                 | <b>psf + king</b>              | <b>1.34</b>               | <b>5.2</b>             | <b>22</b> | <b>143.1</b>               | <b>31.9</b>               | 1.02                       | 5.3                   | 22         | 149.5                       | 33.7                       |
|                   |                                 | bpow remainder                 | 2.08                      | $11.3^{+5.1}_{-3.9}$   | 9         | 174.2                      | 14.4                      | 1.55                       | $11.2^{+5.0}_{-3.9}$  | 11         | 181.5                       | 18.5                       |
|                   |                                 | king remainder                 | 1.78                      | $9.6^{+4.1}_{-2.6}$    | 10        | 174.2                      | 15.5                      | 1.34                       | $9.7^{+4.2}_{-2.6}$   | 11         | 181.5                       | 17.4                       |
| 3C215 (800753a01) | 20                              | psf                            | 6.76                      | —                      | —         | —                          | —                         | 5.10                       | —                     | —          | —                           | —                          |
|                   |                                 | psf + bpow                     | 3.71                      | $6.3^{+3.0}_{-0.7}$    | 29        | 131.4                      | 43.3                      | 2.82                       | $6.3^{+3.0}_{-0.7}$   | 31 ± 13    | 137.3                       | $50.2 \pm 19.1$            |
|                   |                                 | psf + king                     | 2.17                      | $5.0^{+1.2}_{-0.8}$    | 41        | 108.1                      | 59.9                      | 1.73                       | $5.0^{+1.2}_{-0.8}$   | 41         | 112.9                       | 63.2                       |
|                   |                                 | bpow remainder                 | 3.34                      | $8.5^{+1.1}_{-2.4}$    | 25 ± 8    | 140.3                      | $36.8 \pm 11.9$           | 2.63                       | $8.2^{+1.3}_{-2.2}$   | 27 ± 10    | 146.2                       | $43.7 \pm 14.9$            |
|                   |                                 | king remainder                 | 2.34                      | $7.0^{+1.2}_{-0.9}$    | 25 ± 12   | 140.3                      | 38.7                      | 1.88                       | $7.0^{+1.2}_{-0.9}$   | 26 ± 12    | 146.2                       | 41.8                       |
| 3C215 (800753n00) | no correction                   | psf                            | 1.20                      | —                      | —         | —                          | —                         | 1.00                       | —                     | —          | —                           | —                          |
|                   |                                 | psf + bpow                     | 0.24                      | 23.0                   | 9         | 170.8                      | 13.3                      | 0.38                       | 18.8                  | 10         | 178.0                       | 15.7                       |
|                   |                                 | psf + king                     | 0.25                      | 24.3                   | 8         | 178.3                      | 11.4                      | 0.36                       | $19.8^{+12.4}_{-9.4}$ | 9          | 179.6                       | 14.0                       |
|                   |                                 | bpow remainder                 | 0.23                      | 23.7                   | 8         | 173.8                      | 12.8                      | 0.36                       | 19.1                  | 9          | 181.1                       | 15.1                       |
|                   |                                 | king remainder                 | 0.22                      | $24.6^{+23.5}_{-11.4}$ | 7         | 173.8                      | 11.3                      | 0.34                       | $20.3^{+12.1}_{-8.8}$ | 9          | 181.1                       | 13.8                       |
| 3C215 (800753n00) | 10                              | psf                            | 0.60                      | —                      | —         | —                          | —                         | 0.49                       | —                     | —          | —                           | —                          |
|                   |                                 | psf + bpow                     | 0.41                      | 6.3                    | 11        | 160.1                      | 16.0                      | 0.33                       | 6.2                   | 13         | 166.7                       | 19.3                       |
|                   |                                 | psf + king                     | 0.33                      | 4.2                    | 18        | 145.7                      | 26.0                      | 0.29                       | 4.5                   | 17         | 154.9                       | 25.1                       |
|                   |                                 | bpow remainder                 | 0.37                      | 7.7                    | 9         | 164.1                      | 13.8                      | 0.31                       | 8.8                   | 11         | 171.0                       | 16.4                       |
|                   |                                 | king remainder                 | 0.32                      | $7.0^{+8.6}_{-3.4}$    | 9         | 170.3                      | 13.6                      | 0.28                       | $7.3^{+9.0}_{-3.5}$   | 10         | 171.0                       | 14.8                       |
| 3C215 (800718n00) | no correction                   | psf                            | 4.16                      | —                      | —         | —                          | —                         | 3.24                       | —                     | —          | —                           | —                          |
|                   |                                 | psf + bpow                     | 3.19                      | $8.7^{+2.8}_{-3.4}$    | 13        | 206.0                      | 24.0                      | 2.23                       | 8.7                   | 15         | 214.6                       | 29.3                       |
|                   |                                 | psf + king                     | 2.58                      | $4.8^{+2.0}_{-0.9}$    | 22        | 182.3                      | 41.7                      | 1.88                       | $5.2^{+1.9}_{-1.2}$   | 20         | 194.6                       | 40.4                       |
|                   |                                 | bpow remainder                 | 2.85                      | $8.7^{+2.8}_{-2.6}$    | 12 ± 5    | 208.0                      | $22.7 \pm 10.2$           | 2.07                       | $8.7^{+2.8}_{-2.6}$   | 14 ± 6     | 216.8                       | $28.0 \pm 12.6$            |
|                   |                                 | king remainder                 | 2.49                      | $6.6^{+2.1}_{-1.3}$    | 13        | 208.0                      | 25.9                      | 1.85                       | $6.8^{+2.0}_{-1.3}$   | 14         | 216.8                       | 28.2                       |
| 3C215 (800718n00) | 5                               | psf                            | 3.91                      | —                      | —         | —                          | —                         | 3.06                       | —                     | —          | —                           | —                          |
|                   |                                 | psf + bpow                     | 3.10                      | 8.7                    | 13        | 210.0                      | 24.9                      | 2.27                       | 8.7                   | 15         | 218.7                       | 29.3                       |
|                   |                                 | psf + king                     | 2.57                      | $4.5^{+2.2}_{-1.0}$    | 24        | 181.5                      | 46.1                      | 1.99                       | $4.7^{+2.3}_{-1.2}$   | 23         | 192.4                       | 46.3                       |
|                   |                                 | bpow remainder                 | 2.76                      | $8.8^{+3.2}_{-3.2}$    | 12 ± 7    | 212.9                      | $23.2 \pm 12.8$           | 2.10                       | $8.8^{+3.2}_{-3.2}$   | 14 ± 8     | 221.9                       | $28.7 \pm 15.8$            |
|                   |                                 | king remainder                 | 2.49                      | $6.8^{+2.1}_{-1.5}$    | 13        | 212.9                      | 25.8                      | 1.96                       | $6.9^{+2.1}_{-1.6}$   | 14         | 221.9                       | 28.1                       |
| 3C254             | no correction                   | psf                            | 5.94                      | —                      | —         | —                          | —                         | 4.90                       | —                     | —          | —                           | —                          |
|                   |                                 | psf + bpow                     | 4.69                      | 6.3                    | 18        | 412.2                      | 77.5                      | 3.61                       | 6.4                   | 21         | 427.2                       | 97.6                       |
|                   |                                 | psf + king                     | 3.75                      | 5.6                    | 22        | 387.2                      | 95.2                      | 3.18                       | 5.8                   | 22         | 406.3                       | 100.8                      |
|                   |                                 | bpow remainder                 | 4.18                      | $6.3^{+1.6}_{-0.6}$    | 19 ± 5    | 404.3                      | $82.2 \pm 19.8$           | 3.33                       | $6.2^{+1.8}_{-0.5}$   | 22 ± 6     | 421.3                       | $99.7 \pm 25.6$            |
|                   |                                 | king remainder                 | 3.37                      | $6.0^{+1.1}_{-0.8}$    | 20 ± 9    | 454.5                      | 82.4                      | 2.95                       | $6.1^{+1.1}_{-0.8}$   | 20 ± 10    | 421.3                       | 91.6                       |
| 3C254             | 5                               | psf                            | 2.58                      | —                      | —         | —                          | —                         | 2.46                       | —                     | —          | —                           | —                          |
|                   |                                 | psf + bpow                     | 1.37                      | $11.3^{+3.9}_{-7.5}$   | 16        | 413.4                      | 67.5                      | 1.51                       | $11.2^{+4.0}_{-7.5}$  | 19         | 429.8                       | 86.2                       |

**Table 2** – *continued*

| Quasar | phase interval<br>of correction | model<br>outer radius (arcsec) | reduced- $\chi^2$<br>(50) | $R$<br>(50)           | %<br>(50)    | $L_X^{\text{QSO}}$<br>(50) | $L_X^{\text{cl}}$<br>(50) | reduced- $\chi^2$<br>(100) | $R$<br>(100)          | %<br>(100) | $L_X^{\text{QSO}}$<br>(100) | $L_X^{\text{cl}}$<br>(100) |
|--------|---------------------------------|--------------------------------|---------------------------|-----------------------|--------------|----------------------------|---------------------------|----------------------------|-----------------------|------------|-----------------------------|----------------------------|
| 3C254  | 10                              | psf + king                     | 1.28                      | $7.2^{+7.3}_{-3.2}$   | 19           | 394.1                      | 77.9                      | 1.50                       | 8.8                   | 18         | 423.1                       | 77.8                       |
|        |                                 | bpow remainder                 | 1.34                      | $11.5^{+6.1}_{-2.9}$  | 14 ± 6       | 438.6                      | 61.1 ± 26.5               | 1.48                       | $11.9^{+5.9}_{-3.1}$  | 17 ± 7     | 457.1                       | 77.8 ± 33.1                |
|        |                                 | king remainder                 | 1.25                      | $11.8^{+7.6}_{-3.9}$  | 13           | 438.6                      | 54.8                      | 1.44                       | $13.0^{+9.6}_{-4.6}$  | 14         | 457.1                       | 64.4                       |
|        |                                 | <b>psf</b>                     | <b>1.82</b>               | —                     | —            | —                          | —                         | 1.94                       | —                     | —          | —                           | —                          |
|        |                                 | <b>psf + bpow</b>              | <b>0.71</b>               | <b>11.2</b>           | <b>15</b>    | <b>423.6</b>               | <b>63.3</b>               | 1.14                       | 11.3                  | 17         | 441.1                       | 79.5                       |
|        |                                 | <b>psf + king</b>              | <b>0.70</b>               | $12.8^{+11.6}_{-8.7}$ | <b>12</b>    | <b>433.4</b>               | <b>52.1</b>               | 1.13                       | $15.1^{+11.6}_{-8.3}$ | 14         | 455.6                       | 61.3                       |
|        |                                 | bpow remainder                 | 0.75                      | $13.8^{+9.2}_{-4.8}$  | 12           | 454.6                      | 47.0                      | 1.14                       | 13.8                  | 14         | 473.7                       | 66.7                       |
|        |                                 | king remainder                 | 0.68                      | $16.2^{+11.2}_{-6.5}$ | 11           | 454.6                      | 46.5                      | 1.07                       | $17.8^{+10.8}_{-7.2}$ | 13         | 473.7                       | 58.7                       |
| 3C273  | no correction                   | psf                            | 193.30                    | —                     | —            | —                          | —                         | 152.36                     | —                     | —          | —                           | —                          |
|        |                                 | psf + bpow                     | 54.92                     | $2.5^{+0.2}_{-0.2}$   | 8 ± 1        | 1578.1                     | 121.4 ± 11.8              | 78.40                      | 1.2                   | 9          | 1646.2                      | 133.0                      |
|        |                                 | psf + king                     | 33.83                     | $3.1^{+0.1}_{-0.1}$   | 15           | 1457.3                     | 213.8                     | 32.29                      | $3.0^{+0.1}_{-0.1}$   | 15         | 1507.1                      | 229.4                      |
|        |                                 | bpow remainder                 | 54.06                     | $8.7^{+0.3}_{-0.1}$   | 4 ± 1        | 1652.8                     | 66.3 ± 2.4                | 81.69                      | $8.7^{+0.1}_{-0.1}$   | 4 ± 1      | 1722.3                      | 62.9 ± 2.0                 |
|        |                                 | king remainder                 | 46.62                     | $9.1^{+0.4}_{-0.4}$   | 4            | 1652.8                     | 62.1                      | 52.00                      | $8.3^{+0.4}_{-0.3}$   | 4          | 1722.3                      | 68.2                       |
| 3C273  | 5                               | psf                            | 84.32                     | —                     | —            | —                          | —                         | 65.80                      | —                     | —          | —                           | —                          |
|        |                                 | psf + bpow                     | 34.46                     | $8.7^{+0.1}_{-0.6}$   | 5 ± 1        | 1598.3                     | 72.4 ± 5.5                | 41.24                      | $8.7^{+0.1}_{-1.4}$   | 5 ± 1      | 1669.0                      | 68.9                       |
|        |                                 | psf + king                     | 20.89                     | $4.8^{+0.4}_{-0.4}$   | 9            | 1529.4                     | 127.3                     | 18.95                      | $4.2^{+0.3}_{-0.2}$   | 11         | 1561.7                      | 156.5                      |
|        |                                 | bpow remainder                 | 30.68                     | 8.7                   | 5            | 1594.9                     | 73.0                      | 38.13                      | $8.0^{+0.8}_{-1.4}$   | 5 ± 1      | 1661.9                      | 72.4 ± 14.8                |
|        |                                 | king remainder                 | 21.03                     | $6.6^{+0.4}_{-0.3}$   | 6            | 1594.9                     | 85.3                      | 20.92                      | $6.4^{+0.4}_{-0.3}$   | 6          | 1661.9                      | 90.8                       |
| 3C273  | 10                              | psf                            | 78.35                     | —                     | —            | —                          | —                         | 61.61                      | —                     | —          | —                           | —                          |
|        |                                 | psf + bpow                     | 27.74                     | $8.7^{+0.1}_{-0.6}$   | 5 ± 1        | 1575.5                     | 71.3 ± 5.0                | 36.43                      | $8.7^{+0.1}_{-1.3}$   | 5          | 1645.2                      | 68.0                       |
|        |                                 | psf + king                     | 15.11                     | $3.7^{+0.3}_{-0.2}$   | 12           | 1451.2                     | 173.4                     | 14.37                      | $3.5^{+0.2}_{-0.2}$   | 13         | 1490.6                      | 196.8                      |
|        |                                 | bpow remainder                 | 24.82                     | $8.8^{+0.1}_{-0.3}$   | 5 ± 1        | 1584.9                     | 69.1 ± 3.2                | 33.68                      | $8.7^{+0.1}_{-0.6}$   | 5 ± 1      | 1651.4                      | 66.4 ± 4.9                 |
|        |                                 | king remainder                 | 17.72                     | $7.3^{+0.5}_{-0.4}$   | 5            | 1584.9                     | 75.1                      | 18.98                      | $7.0^{+0.4}_{-0.4}$   | 5          | 1651.4                      | 80.7                       |
| 3C273  | 20                              | <b>psf</b>                     | <b>75.49</b>              | —                     | —            | —                          | —                         | 59.81                      | —                     | —          | —                           | —                          |
|        |                                 | <b>psf + bpow</b>              | <b>27.14</b>              | $8.7^{+0.1}_{-0.7}$   | <b>5 ± 1</b> | <b>1572.1</b>              | <b>69.2 ± 5.3</b>         | 36.21                      | $8.7^{+0.1}_{-1.5}$   | 4 ± 1      | 1641.6                      | 65.7 ± 10.9                |
|        |                                 | <b>psf + king</b>              | <b>16.20</b>              | $4.5^{+0.5}_{-0.4}$   | <b>9 ±</b>   | <b>1495.6</b>              | <b>130.2 ±</b>            | 15.87                      | $3.9^{+0.3}_{-0.2}$   | 11         | 1521.1                      | 164.7                      |
|        |                                 | bpow remainder                 | 24.16                     | $8.7^{+0.1}_{-0.5}$   | 5 ± 1        | 1576.7                     | 68.4                      | 33.42                      | $8.7^{+0.1}_{-1.0}$   | 4          | 1642.9                      | 65.3                       |
|        |                                 | king remainder                 | 17.11                     | $7.1^{+0.5}_{-0.4}$   | 5            | 1576.7                     | 75.4                      | 18.72                      | $6.8^{+0.4}_{-0.4}$   | 5          | 1642.9                      | 80.8                       |
| 3C273  | 40                              | psf                            | 77.25                     | —                     | —            | —                          | —                         | 60.91                      | —                     | —          | —                           | —                          |
|        |                                 | psf + bpow                     | 27.55                     | $8.7^{+0.1}_{-0.7}$   | 5 ± 1        | 1570.3                     | 70.2 ± 5.3                | 36.62                      | $8.7^{+0.1}_{-1.6}$   | 5 ± 1      | 1639.6                      | 66.7 ± 11.5                |
|        |                                 | psf + king                     | 16.20                     | $4.2^{+0.5}_{-0.4}$   | 10           | 1482.2                     | 141.0                     | 15.57                      | $3.7^{+0.3}_{-0.2}$   | 12         | 1504.7                      | 174.0                      |
|        |                                 | bpow remainder                 | 24.56                     | $8.7^{+0.1}_{-0.4}$   | 5 ± 1        | 1576.0                     | 69.1 ± 3.6                | 33.82                      | $8.7^{+0.1}_{-0.9}$   | 5 ± 1      | 1642.2                      | 66.0 ± 6.4                 |
|        |                                 | king remainder                 | 17.46                     | $7.2^{+0.5}_{-0.4}$   | 5            | 1576.0                     | 75.8                      | 18.90                      | $6.9^{+0.4}_{-0.4}$   | 5          | 1642.2                      | 81.4                       |
| 3C273  | 80                              | psf                            | 81.73                     | —                     | —            | —                          | —                         | 64.04                      | —                     | —          | —                           | —                          |
|        |                                 | psf + bpow                     | 31.38                     | $8.7^{+0.1}_{-0.6}$   | 5 ± 2        | 1568.6                     | 71.3 ± 5.0                | 38.95                      | $8.7^{+0.1}_{-1.3}$   | 5 ± 1      | 1637.8                      | 68.0 ± 9.7                 |
|        |                                 | psf + king                     | 19.03                     | $4.0^{+0.4}_{-0.3}$   | 11           | 1465.0                     | 155.4                     | 17.18                      | $3.6^{+0.2}_{-0.2}$   | 13         | 1497.6                      | 184.2                      |
|        |                                 | bpow remainder                 | 27.98                     | $8.7^{+0.1}_{-0.4}$   | 5 ± 1        | 1575.3                     | 70.17 ± 3.5               | 35.98                      | $8.7^{+0.1}_{-0.8}$   | 5 ± 1      | 1641.6                      | 67.0 ± 5.6                 |

Table 2 – *continued*

| Quasar            | phase interval of correction | model outer radius (arcsec) | reduced- $\chi^2$ (50) | $R$ (50)              | % (50)      | $L_X^{\text{QSO}}$ (50) | $L_X^{\text{cl}}$ (50) | reduced- $\chi^2$ (100) | $R$ (100)              | % (100)                       | $L_X^{\text{QSO}}$ (100) | $L_X^{\text{cl}}$ (100)           |
|-------------------|------------------------------|-----------------------------|------------------------|-----------------------|-------------|-------------------------|------------------------|-------------------------|------------------------|-------------------------------|--------------------------|-----------------------------------|
|                   |                              | king remainder              | 20.58                  | $7.2^{+0.4}_{-0.4}$   | 5           | 1575.3                  | 76.8                   | 20.88                   | $6.9^{+0.4}_{-0.4}$    | 6                             | 1641.6                   | 82.4                              |
| 3C275.1           | no correction                | psf                         | 1.71                   | —                     | —           | —                       | —                      | 1.40                    | —                      | —                             | —                        | —                                 |
|                   |                              | psf + bpow                  | 0.81                   | $18.7^{+12.1}_{-6.1}$ | $16 \pm 7$  | 111.0                   | $17.9 \pm 8.2$         | 0.69                    | $18.7^{+11.5}_{-6.0}$  | $19 \pm 10$                   | 115.8                    | $23.5 \pm 11.5$                   |
|                   |                              | psf + king                  | 0.81                   | $21.3^{+14.7}_{-8.3}$ | 14          | 113.8                   | 16.1                   | 0.70                    | $21.6^{+12.7}_{-8.0}$  | 17                            | 118.7                    | 21.1                              |
|                   |                              | bpow remainder              | 1.08                   | 20.0                  | 12          | 124.0                   | 14.5                   | 0.89                    | $20.5^{+33.3}_{-5.6}$  | $15 \pm 11$                   | 129.2                    | $19.5 \pm 14.3$                   |
|                   |                              | king remainder              | 0.95                   | $25.5^{+19.7}_{-9.3}$ | 12          | 124.0                   | 14.4                   | 0.80                    | $25.3^{+15.2}_{-8.8}$  | 15                            | 129.2                    | 19.7                              |
| 3C275.1           | 5                            | <b>psf</b>                  | 2.02                   | —                     | —           | —                       | —                      | <b>1.61</b>             | —                      | —                             | —                        | —                                 |
|                   |                              | psf + bpow                  | —                      | —                     | —           | —                       | —                      | <b>1.13</b>             | $37.2^{+20.5}_{-15.4}$ | <b>25 <math>\pm</math> 13</b> | <b>111.1</b>             | <b>32.4 <math>\pm</math> 16.2</b> |
|                   |                              | <b>psf + king</b>           | 1.47                   | 46.1                  | 17          | 110.5                   | 19.7                   | <b>1.12</b>             | $35.4^{+20.5}_{-14.2}$ | <b>23 <math>\pm</math></b>    | <b>114.6</b>             | <b>29.4 <math>\pm</math></b>      |
|                   |                              | bpow remainder              | —                      | —                     | —           | —                       | —                      | 1.04                    | $37.7^{+29.7}_{-15.8}$ | $25 \pm 13$                   | 112.3                    | $32.1 \pm 15.5$                   |
|                   |                              | king remainder              | 1.04                   | 44.1                  | 18          | 107.8                   | 20.0                   | 1.04                    | $34.8^{+19.6}_{-14.0}$ | 24                            | 112.3                    | 29.6                              |
| 3C281 (800635n00) | no correction                | psf                         | 12.44                  | —                     | —           | —                       | —                      | 9.39                    | —                      | —                             | —                        | —                                 |
|                   |                              | psf + bpow                  | 7.68                   | $6.3^{+2.8}_{-0.3}$   | $62 \pm 23$ | 91.9                    | $128.0 \pm 39.6$       | 5.24                    | $6.3^{+2.8}_{-0.3}$    | $66 \pm 26$                   | 94.4                     | $154.7 \pm 48.7$                  |
|                   |                              | psf + king                  | 4.07                   | $5.3^{+0.7}_{-0.5}$   | 83          | 42.9                    | 172.6                  | 3.09                    | $5.5^{+0.7}_{-0.6}$    | 81                            | 50.3                     | 179.4                             |
|                   |                              | bpow remainder              | 7.09                   | $8.7^{+0.9}_{-0.9}$   | $47 \pm 8$  | 30.9                    | $97.4 \pm 14.4$        | 5.04                    | $8.7^{+1.0}_{-0.8}$    | $51 \pm 9$                    | 136.4                    | $118.5 \pm 18.5$                  |
|                   |                              | king remainder              | 4.96                   | $7.5^{+0.8}_{-0.7}$   | 49          | 130.9                   | 105.9                  | 3.73                    | $7.6^{+0.9}_{-0.6}$    | 50                            | 136.4                    | 116.7                             |
| 3C281 (800635n00) | 5                            | psf                         | 3.78                   | —                     | —           | —                       | —                      | 2.99                    | —                      | —                             | —                        | —                                 |
|                   |                              | psf + bpow                  | 2.72                   | $6.3^{+5.1}_{-1.0}$   | 47          | 147.4                   | 108.9                  | 2.11                    | $6.3^{+5.1}_{-1.0}$    | 50                            | 154.1                    | 129.2                             |
|                   |                              | psf + king                  | 1.79                   | $5.1^{+1.8}_{-1.0}$   | 67          | 91.8                    | 155.6                  | 1.49                    | $5.1^{+1.9}_{-1.0}$    | 67                            | 97.2                     | 164.0                             |
|                   |                              | bpow remainder              | 2.50                   | $9.2^{+3.4}_{-3.1}$   | $36 \pm 19$ | 179.2                   | $85.3 \pm 41.8$        | 2.00                    | $9.1^{+3.5}_{-3.1}$    | $40 \pm 22$                   | 186.8                    | $103.6 \pm 52.4$                  |
|                   |                              | king remainder              | 1.91                   | $7.5^{+2.1}_{-1.3}$   | 28          | 179.2                   | 91.7                   | 1.59                    | $7.6^{+2.1}_{-1.3}$    | 39                            | 186.8                    | 100.5                             |
| 3C281 (800635a01) | no correction                | psf                         | 11.36                  | —                     | —           | —                       | —                      | 8.20                    | —                      | —                             | —                        | —                                 |
|                   |                              | psf + bpow                  | 5.24                   | $6.3^{+2.0}_{-0.3}$   | $48 \pm 13$ | 163.0                   | $126.1 \pm 31.1$       | 4.06                    | $6.3^{+2.0}_{-0.4}$    | $49 \pm 14$                   | 174.4                    | $139.5 \pm 36.0$                  |
|                   |                              | psf + king                  | 2.75                   | $5.3^{+0.9}_{-0.6}$   | 61          | 118.3                   | 158.6                  | 2.00                    | $5.2^{+0.8}_{-0.6}$    | 62                            | 121.1                    | 168.9                             |
|                   |                              | bpow remainder              | 4.91                   | $8.7^{+0.6}_{-1.3}$   | $38 \pm 7$  | 197.0                   | $100.3 \pm 16.5$       | 3.89                    | $8.7^{+0.5}_{-1.6}$    | $40 \pm 8$                    | 205.2                    | $116.8 \pm 22.5$                  |
|                   |                              | king remainder              | 3.34                   | $7.5^{+0.9}_{-0.7}$   | 38          | 197.0                   | 102.6                  | 2.50                    | $7.5^{+0.9}_{-0.7}$    | 39                            | 60.3                     | 110.5                             |
| 3C281 (800635a01) | 5                            | <b>psf</b>                  | <b>3.79</b>            | —                     | —           | —                       | —                      | 3.16                    | —                      | —                             | —                        | —                                 |
|                   |                              | <b>psf + bpow</b>           | <b>1.39</b>            | $6.7^{+3.4}_{-1.3}$   | <b>42</b>   | <b>189.5</b>            | <b>118.5</b>           | 1.86                    | $6.3^{+3.7}_{-1.0}$    | 43                            | 201.8                    | 127.1                             |
|                   |                              | <b>psf + king</b>           | <b>0.72</b>            | $5.0^{+2.1}_{-1.1}$   | <b>56</b>   | <b>138.6</b>            | <b>152.6</b>           | 1.11                    | $4.8^{+1.8}_{-0.9}$    | 60                            | 133.1                    | 167.9                             |
|                   |                              | bpow remainder              | 1.32                   | $8.8^{+2.5}_{-1.8}$   | $33 \pm 11$ | 223.3                   | $93.8 \pm 28.9$        | 1.75                    | $8.5^{+2.8}_{-1.5}$    | $35 \pm 13$                   | 233.0                    | $106.0 \pm 35.3$                  |
|                   |                              | king remainder              | 0.94                   | $8.1^{+1.9}_{-1.4}$   | 33          | 223.6                   | 91.7                   | 1.27                    | $7.7^{+1.8}_{-1.3}$    | 33                            | 233.0                    | 97.5                              |
| 3C334             | no correction                | psf                         | 3.79                   | —                     | —           | —                       | —                      | 3.20                    | —                      | —                             | —                        | —                                 |
|                   |                              | psf + bpow                  | 3.06                   | 6.3                   | 13          | 360.6                   | 41.3                   | 2.64                    | 6.3                    | 14                            | 376.2                    | 47.8                              |
|                   |                              | psf + king                  | 2.30                   | 5.3                   | 17          | 339.4                   | 55.8                   | 2.11                    | 5.3                    | 17                            | 353.8                    | 58.9                              |
|                   |                              | bpow remainder              | 2.72                   | $6.3^{+2.8}_{-1.1}$   | $13 \pm 5$  | 357.6                   | $42.9 \pm 16.8$        | 2.44                    | $6.3^{+2.8}_{-1.2}$    | $14 \pm 6$                    | 372.6                    | $50.0 \pm 20.3$                   |

**Table 2** – *continued*

| Quasar      | phase interval<br>of correction | model<br>outer radius (arcsec) | reduced- $\chi^2$<br>(50) | $R$<br>(50)           | %<br>(50)                    | $L_X^{\text{QSO}}$<br>(50) | $L_X^{\text{cl}}$<br>(50)          | reduced- $\chi^2$<br>(100) | $R$<br>(100)         | %<br>(100) | $L_X^{\text{QSO}}$<br>(100) | $L_X^{\text{cl}}$<br>(100) |
|-------------|---------------------------------|--------------------------------|---------------------------|-----------------------|------------------------------|----------------------------|------------------------------------|----------------------------|----------------------|------------|-----------------------------|----------------------------|
|             |                                 | king remainder                 | 2.10                      | $6.0^{+1.5}_{-1.0}$   | 14                           | 357.6                      | 45.1                               | 1.99                       | $6.0^{+1.5}_{-1.0}$  | 14         | 372.6                       | 48.1                       |
| 3C334       | 5                               | <b>psf</b>                     | <b>1.43</b>               | —                     | —                            | —                          | —                                  | 1.40                       | —                    | —          | —                           | —                          |
|             |                                 | <b>psf + bpow</b>              | <b>1.14</b>               | <b>10.3</b>           | <b>8</b>                     | <b>385.1</b>               | <b>28.4</b>                        | 1.20                       | 9.9                  | 10         | 400.9                       | 34.7                       |
|             |                                 | <b>psf + king</b>              | <b>0.77</b>               | <b>4.6</b>            | <b>17</b>                    | <b>345.6</b>               | <b>57.7</b>                        | 0.94                       | 4.6                  | 18         | 359.6                       | 61.2                       |
|             |                                 | bpow remainder                 | 1.01                      | 11.2                  | 8                            | 388.7                      | 26.8                               | 1.11                       | 11.2                 | 9          | 405.0                       | 32.0                       |
|             |                                 | king remainder                 | 0.80                      | $7.5^{+4.2}_{-2.6}$   | 9                            | 388.7                      | 30.9                               | 0.95                       | $7.5^{+4.3}_{-2.6}$  | 9          | 405.0                       | 33.7                       |
| 3C334       | 20                              | psf                            | 4.14                      | —                     | —                            | —                          | —                                  | 3.15                       | —                    | —          | —                           | —                          |
|             |                                 | psf + bpow                     | 3.66                      | 6.3                   | 16                           | 351.9                      | 54.8                               | 2.73                       | 6.3                  | 17         | 368.6                       | 61.6                       |
|             |                                 | psf + king                     | 2.94                      | 5.4                   | 22                           | 327.0                      | 72.6                               | 2.19                       | 5.4                  | 22         | 340.5                       | 76.9                       |
|             |                                 | bpow remainder                 | 3.27                      | $6.3^{+2.5}_{-1.0}$   | $18 \pm 6$                   | 341.7                      | $58.8 \pm 20.8$                    | 2.53                       | $6.2^{+2.5}_{-1.0}$  | $20 \pm 7$ | 356.0                       | $69.9 \pm 25.2$            |
|             |                                 | king remainder                 | 2.64                      | $5.8^{+1.3}_{-1.0}$   | 19                           | 341.7                      | 64.1                               | 2.04                       | $5.8^{+1.3}_{-1.0}$  | 19         | 356.0                       | 68.0                       |
| H1821 + 643 | no corr                         | psf                            | 87.37                     | —                     | —                            | —                          | —                                  | 108.64                     | —                    | —          | —                           | —                          |
|             |                                 | psf + bpow                     | 4.58                      | $34.0^{+2.5}_{-2.4}$  | $15 \pm 1$                   | 899.1                      | $126.1 \pm 5.7$                    | 15.10                      | $40.3^{+2.0}_{-1.9}$ | $21 \pm 1$ | 937.8                       | $202.6 \pm 9.5$            |
|             |                                 | psf + king                     | 3.70                      | $27.4^{+1.9}_{-1.7}$  | 13                           | 915.6                      | 110.7                              | 16.49                      | $39.5^{+2.1}_{-2.0}$ | 19         | 965.2                       | 179.2                      |
|             |                                 | bpow remainder                 | 6.33                      | $28.3^{+1.8}_{-1.7}$  | $14 \pm 1$                   | 944.4                      | $122.5 \pm 6.9$                    | 15.46                      | $41.6^{+2.1}_{-2.0}$ | $20 \pm 1$ | 984.2                       | $195.1 \pm 9.1$            |
|             |                                 | king remainder                 | 4.21                      | $28.5^{+1.9}_{-1.8}$  | 13                           | 944.4                      | 107.5                              | 15.48                      | $40.1^{+2.2}_{-2.0}$ | 18         | 984.2                       | 177.3                      |
| H1821 + 643 | 5                               | psf                            | 14.56                     | —                     | —                            | —                          | —                                  | 19.47                      | —                    | —          | —                           | —                          |
|             |                                 | psf + bpow                     | 2.02                      | $38.4^{+8.3}_{-6.4}$  | $12 \pm 1$                   | 985.1                      | $111.6 \pm 12.5$                   | 2.85                       | $81.3^{+5.0}_{-3.5}$ | $19 \pm 1$ | 1034.1                      | $194.9 \pm 12.5$           |
|             |                                 | psf + king                     | 2.00                      | $36.2^{+7.6}_{-5.7}$  | 11                           | 1005.6                     | 94.2                               | 3.60                       | $52.3^{+7.8}_{-6.4}$ | 17         | 1056.3                      | 171.9                      |
|             |                                 | bpow remainder                 | 2.76                      | $40.7^{+17.7}_{-7.0}$ | 11                           | 1054.8                     | 102.5                              | 3.20                       | $81.2^{+5.9}_{-3.3}$ | $17 \pm 1$ | 1099.1                      | $184.5 \pm 12.7$           |
|             |                                 | king remainder                 | 2.26                      | $38.6^{+8.5}_{-6.2}$  | 10                           | 1054.8                     | 89.8                               | 3.57                       | $54.3^{+8.3}_{-6.7}$ | 16         | 1099.1                      | 167.7                      |
| H1821 + 643 | 10                              | psf                            | 14.66                     | —                     | —                            | —                          | —                                  | 19.73                      | —                    | —          | —                           | —                          |
|             |                                 | psf + bpow                     | 2.41                      | 37.1                  | 12                           | 911.5                      | 102.4                              | 3.11                       | $81.3^{+4.5}_{-3.8}$ | $19 \pm 1$ | 956.8                       | $180.5 \pm 11.6$           |
|             |                                 | psf + king                     | 2.44                      | $34.9^{+7.2}_{-5.5}$  | 10                           | 920.0                      | 86.5                               | 3.94                       | $53.3^{+8.1}_{-6.6}$ | 17         | 977.6                       | 159.0                      |
|             |                                 | bpow remainder                 | 2.85                      | $38.9^{+10.5}_{-6.8}$ | $11 \pm 1$                   | 966.8                      | $95.4 \pm 11.2$                    | 3.28                       | $81.3^{+5.2}_{-3.7}$ | $18 \pm 1$ | 1007.4                      | $172.2 \pm 11.8$           |
|             |                                 | king remainder                 | 2.49                      | $36.8^{+7.8}_{-5.8}$  | 10                           | 966.7                      | 83.2                               | 3.77                       | $54.7^{+8.5}_{-6.8}$ | 16         | 1007.4                      | 156.1                      |
| H1821 + 643 | 20                              | <b>psf</b>                     | <b>14.51</b>              | —                     | —                            | —                          | —                                  | 19.49                      | —                    | —          | —                           | —                          |
|             |                                 | <b>psf + bpow</b>              | <b>0.96</b>               | $34.1^{+6.3}_{-8.1}$  | <b><math>13 \pm 2</math></b> | <b>951.6</b>               | <b><math>110.4 \pm 12.8</math></b> | 2.00                       | $81.3^{+6.2}_{-3.7}$ | $19 \pm 1$ | 1001.1                      | $190.0 \pm 12.1$           |
|             |                                 | <b>psf + king</b>              | <b>1.09</b>               | $29.3^{+5.7}_{-4.6}$  | <b>11</b>                    | <b>968.3</b>               | <b>94.8</b>                        | 3.18                       | $50.0^{+8.0}_{-6.5}$ | 17         | 1021.6                      | 166.2                      |
|             |                                 | bpow remainder                 | 0.87                      | $34.5^{+6.2}_{-8.0}$  | $13 \pm 1$                   | 960.2                      | $109.3 \pm 12.2$                   | 1.85                       | $81.2^{+6.1}_{-3.6}$ | $19 \pm 1$ | 1000.7                      | $190.2 \pm 12.1$           |
|             |                                 | king remainder                 | 0.98                      | $29.0^{+5.4}_{-4.5}$  | 11                           | 960.2                      | 95.6                               | 3.00                       | $49.0^{+7.6}_{-6.2}$ | 17         | 1000.7                      | 168.2                      |

Notes:

The best-fitting parameters are presented for each quasar profile fitted first to an outer radius of 50 arcsec, and then 100 arcsec.

 $L_X$  is the X-ray luminosity in the *observed* 0.1–2 keV energy band, expressed in units of  $10^{43}$  erg s $^{-1}$ . $R$  is expressed in arcsec and is either the break in the broken power-law model or the core radius in the King law model.

% shows the fraction of the total luminosity represented by the extended component, with the errors showing its statistical significance.

The bold font marks those fits shown in Fig. 2.

there are significant differences between the PSF-only fit to the profile and the fits that include a model for extended emission. In all this analysis we necessarily assume that any extended component is centred on the quasar (in no case do we see any evidence for a secondary off-centre peak), and derive its properties such as scale and luminosity assuming that it is at the redshift of the quasar.

The present data cannot rule out a contribution to the extended component of X-ray emission from the active nuclei of close companion galaxies to each of the quasars. Such emission would, of course, provide further support for a clustered environment. The probability of obtaining an unassociated X-ray source within an aperture of 1 arcmin<sup>2</sup> centred on a quasar is less than 10<sup>-3</sup>, at the flux level of the extended emission. Thus there is little chance of the extended emission component being caused by contamination by foreground or background sources.

### 3 RESULTS FOR INDIVIDUAL QUASARS

#### 3.1 3C48

Given its proximity to a very luminous source of photoionization, the low-ionization state observed in the spatially extended oxygen line emission around 3C48 led Fabian et al. (1987) to deduce a high-density environment around this quasar. The inferred gas pressure of  $3\text{--}8 \times 10^5 \text{ cm}^{-3} \text{ K}$  within 30 kpc of the quasar core is consistent with confinement of the extended emission-line region by an intracluster medium. There is, however, no strong evidence for a rich cluster of galaxies from optical images (Yee, Green & Stockman 1986; Yates et al. 1989).

The fit to the radial profile is substantially improved by the addition of an extended component, the best fits being obtained in all cases when this is represented by a King law. The extended component requires a very consistent value for the core radius  $R$  of around 5–6 arcsec in all fits (1 arcsec corresponds to 6.2 kpc at the redshift of the quasar<sup>1</sup>), and accounts for 10–16 per cent of the total X-ray source. The full variation of its luminosity is  $5\text{--}10 \times 10^{44} \text{ erg s}^{-1}$ , with most of the values derived being to the lower end of this range.

#### 3.2 3C215

This quasar lies in a densely clustered environment (Ellingson et al. 1991; Hintzen 1984), and the radio source has a very complex structure suggestive of deflection and distortion of the radio jet to the south-east by some external medium. The two sides of the radio source show asymmetric Faraday depolarization, which can be interpreted as resulting from differing lines of sight through a depolarizing cluster medium (Garrington, Conway & Leahy 1991). Crawford & Fabian (1989) inferred a high gas pressure of over  $3 \times 10^5 \text{ cm}^{-3} \text{ K}$  from the ionization state of the extended line emission within 30 kpc of the quasar nucleus.

We have extracted radial profiles from three observations of 3C215. Smearing of the image seems to have badly affected observation number 800753n00, as  $R$  decreases substantially after correction of the image. In all cases, the reduced  $\chi^2$  of the fit improves from the addition of an extended component to the HRI

<sup>1</sup>We assume a value for the Hubble constant of  $H_0 = 50 \text{ km s}^{-1} \text{ Mpc}^{-1}$  and a cosmological deceleration parameter of  $q_0 = 0.5$  throughout this paper.

PSF model, although there is little preference shown between the King and broken power-law models. In the fits allowing free normalization of the PSF component, the  $R$  derived is in the range 4–9 arcsec (where 1 arcsec corresponds to 6.5 kpc at the redshift of the quasar), with the broken power-law model always yielding the larger values of  $R$ . The luminosity of the extended component ranges over  $1.6\text{--}6.3 \times 10^{44} \text{ erg s}^{-1}$ , and accounts for 11–40 per cent of the total X-ray emission from this source; the higher values are derived from the King law models.

#### 3.3 3C254

3C254 is a quasar with a very asymmetric radio source, and was discovered by us (Forbes et al. 1990) to lie in a spectacular emission-line region extending out to radii of 80 kpc. The optical nebula is again at low ionization, with an inferred pressure of  $> 10^6 \text{ cm}^{-3} \text{ K}$  within 30 kpc (Forbes et al. 1990; Crawford & Vanderriest 1997). The kinematics and distribution of the line-emitting gas in combination with the radio morphology strongly suggest that the radio plasma to the east of the quasar is interacting with a dense clumpy environment (Bremer 1997; Crawford & Vanderriest 1997). The radio source itself also shows asymmetric depolarization (Liu & Pooley 1991). Optical continuum images show an overdensity of faint objects around the quasar consistent with a location in a compact cluster or group (Bremer 1997). The HRI image of 3C254 shows a detached secondary source of X-ray emission approximately 35 arcsec east of the quasar, but at a very low fraction of the total quasar luminosity. There is no optical counterpart to this source on the Space Telescope Science Institute Digitized Sky Survey.

The fitting of the profile is improved by the addition of an extended component to the HRI PSF model, although it cannot discriminate between a King or broken power-law model. The extended emission contains 12–19 per cent of the total X-ray luminosity of the source. The characteristic scalelength  $R$  of the extended emission component varies over 9–15 arcsec (1 arcsec corresponds to 8.1 kpc at the redshift of the quasar), with a luminosity of  $5\text{--}9 \times 10^{44} \text{ erg s}^{-1}$ .

#### 3.4 3C273

3C273 is famous for its jet, which can be seen in the outermost contours of our corrected images. The jet is known to emit X-rays at around 16 arcsec (nearer the core than the radio and optical features of the jet), but the emission from the jet contributes less than 0.5 per cent of the total X-ray luminosity of the source associated with the quasar (Harris & Stern 1987). From optical images, 3C273 may be a member of a poor cluster of galaxies (Stockton 1980).

All the wobble-corrected profiles of 3C273 require the addition of an extended component (preferably a King law). Each of the models for the extended emission yields slightly (and consistently) different results: the broken power-law fits tend to have an  $R$  of 8.7 arcsec (where 1 arcsec corresponds to 3.6 kpc at the redshift of the quasar) and contain 5 per cent of the total X-ray luminosity, at  $7 \times 10^{44} \text{ erg s}^{-1}$ . The King law fits show a greater variation in the parameters, but have an  $R$  of only  $\sim 4$  arcsec, and  $\sim 11$  per cent of the total luminosity at  $1.3\text{--}2.0 \times 10^{45} \text{ erg s}^{-1}$ . The extended emission we find in the environs of this quasar is sufficiently luminous that it cannot easily be ascribed to the jet.

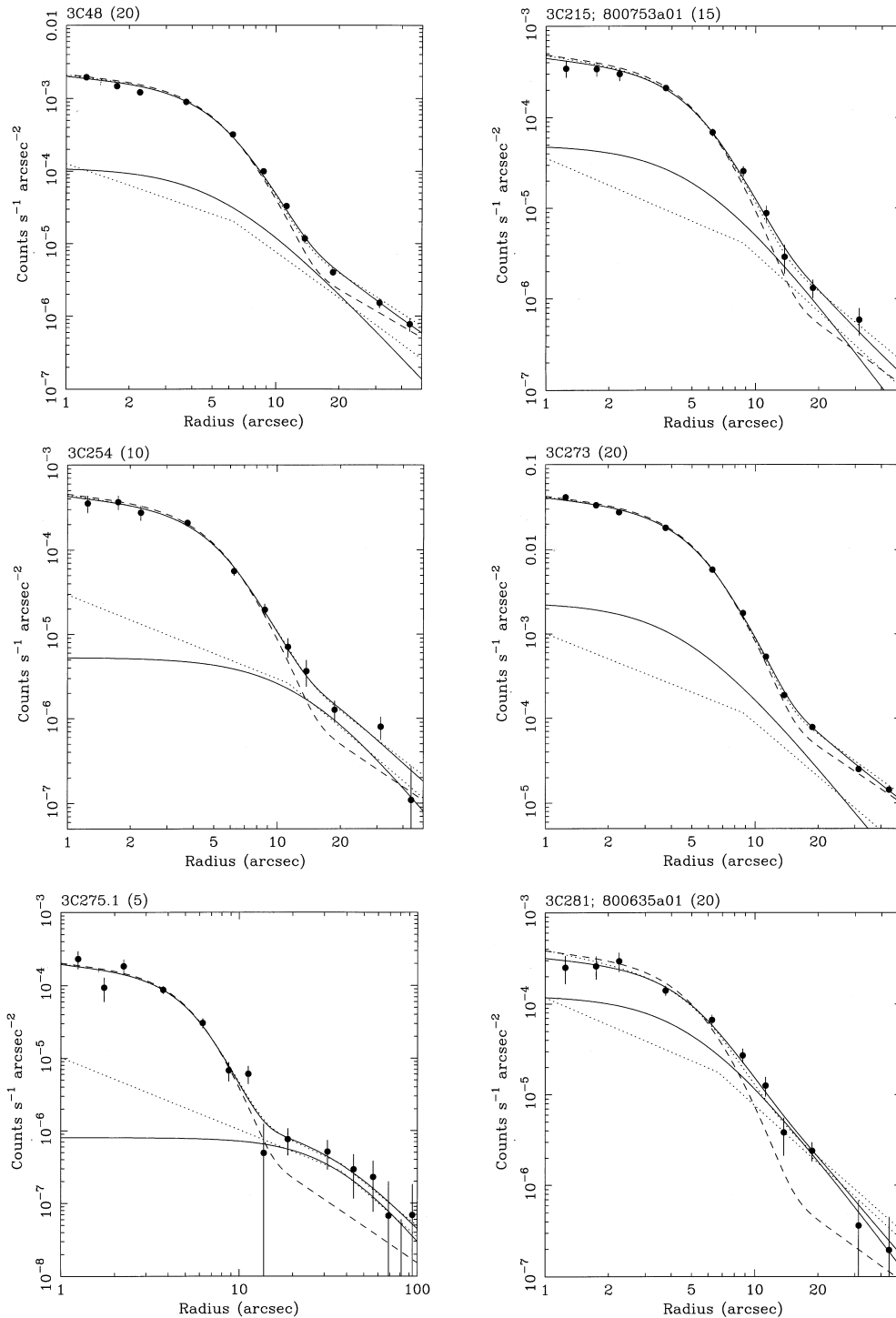


**Figure 2.** The radial profile of the X-ray emission from each of the quasars out to 50 arcsec, with the exception of 3C275.1 where the profile is shown out to 100 arcsec. The phase interval used for this radial profile is shown in brackets after the quasar name in each plot. The data are shown as solid circle markers, with the best fit of the empirical HRI PSF on its own plotted as a dashed line. The best-fitting PSF + King law and PSF + broken power-law models (upper solid and dotted lines respectively) are plotted, as well as just the extended component to each of these fits (the lower solid and dotted lines respectively). The fits shown in these plots are marked by a bold font in Table 2.

### 3.5 3C275.1

3C275.1 was the first quasar discovered from optical galaxy counts to be located at the centre of a rich cluster of galaxies (Hintzen, Boeshaar & Scott 1981; Hintzen 1984; Ellingson et al.

1991). The radio source is only slightly bent, but the two sides display an asymmetry in the Faraday depolarization (Garrington et al. 1991). The quasar is embedded in a host galaxy with a continuum spatial profile and absolute magnitude typical of a bright cluster cD; this is in turn surrounded by a large (100 kpc

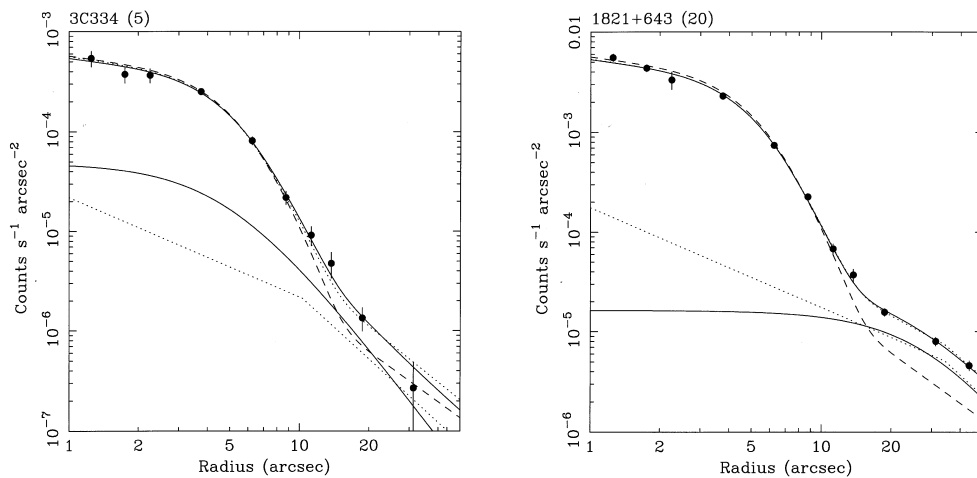


Figure 2 – continued

optical emission-line nebula (Hintzen & Romanishin 1986; Hintzen & Stocke 1986). Crawford & Fabian (1989) deduce a pressure within this gas of  $> 3 \times 10^5 \text{ cm}^{-3} \text{ K}$  at radii of  $< 20 \text{ kpc}$  and thus also the presence of an intracluster medium (Crawford & Fabian 1989). The fit to the X-ray radial profile improves slightly with the addition of an extended component to the HRI PSF. The models all imply a surprisingly broad core, so much so that fitting a second component to data only within a 50 arcsec radius is not robust. The King and broken power-law models yield very similar results, with  $R \sim 36 \text{ arcsec}$  (where 1 arcsec corresponds to 7.4 kpc at the redshift of the quasar), and 24 per cent of the total X-ray luminosity of the source at  $L_X \sim 3 \times 10^{44} \text{ erg s}^{-1}$ .

### 3.6 3C281

3C281 is known to lie in a rich cluster (Yee & Green 1987), and Bremer et al. (1992) infer a pressure exceeding  $2 \times 10^6 \text{ cm}^{-3} \text{ K}$  in the extended emission-line gas within a radius of 20 kpc. After the wobble correction has been applied, the X-ray source associated with the quasar shows a distinct elongation to either side of the core along a position angle of  $45^\circ$  west of north. The direction of this elongation is, however, at odds with that of the radio source which has an axis  $10^\circ$  east of north.

The profiles extracted from both observations of 3C281 both show an improved fit from the addition of an extended component (preferably a King law). The fractional luminosity of this component is high, ranging over 42–67 per cent at  $1.1\text{--}1.7 \times 10^{45} \text{ erg s}^{-1}$  (the higher values obtained with the King model fits). The characteristic radius of this component is 5–6 arcsec (where 1 arcsec corresponds to 7.6 kpc at the redshift of the quasar).

### 3.7 3C334

This quasar lies in a clustered environment (Hintzen 1984) and has a pressure within the extended emission-line region of over  $6 \times 10^5 \text{ cm}^{-3} \text{ K}$  at 30 kpc from the quasar core (Crawford & Fabian 1989). The quasar again shows a depolarization asymmetry (Garrington et al. 1991), and narrow-band imaging by Hes (1995) suggests that the [O II] line emission is extended along the same position angle of  $\sim 150^\circ$  as the strong radio jet to the south-east of the quasar core.

The fits to the wobble-corrected profiles show an improvement

to the fit with the addition of an extended component, preferably a King model. The length-scale  $R$  of this component lies in the range 5–10 arcsec (where 1 arcsec corresponds to 7.4 kpc at the redshift of the quasar), and contains 8–22 per cent of the total X-ray luminosity at  $3\text{--}8 \times 10^{44} \text{ erg s}^{-1}$ .

### 3.8 H1821+643

H1821+643 is a radio-quiet quasar which is luminous in the infrared. The X-ray emission was found to have a significant extended component by Hall et al. (1997). It is included here as a comparison object.

The fits improve dramatically with the inclusion of an extended component. With the 50-arcsec apertures, the King model is often preferred, whereas the 100-arcsec apertures show a marked improvement for the broken power-law model. The characteristic radius of this extended component,  $R$ , shows a wide range of 29–81 arcsec (where 1 arcsec corresponds to 5.5 kpc at the redshift of the quasar), but clear separation according to both extended model and outer profile radius employed. The extended component contains from 10–19 per cent of the X-ray luminosity, at  $8\text{--}20 \times 10^{44} \text{ erg s}^{-1}$ .

## 4 SUMMARY OF RESULTS

We tabulate average properties of the extended emission component from the profile fits to each quasar in Table 3, where these averages are derived only from the fits in which the normalizations of the PSF and model for the extended emission are both allowed to vary (labelled as PSF + broken power-law and PSF + King law in Table 2). The values are averaged from the fits to only the wobble-corrected images (and from each phase interval employed). As is clear from both Tables 2 and 3, where the scatter in properties is sufficiently low for comparison to be made (3C48, 3C215, 3C273 and 3C281), systematic differences can be seen between parameters derived using the King and broken power-law fits. The King law always gives a higher X-ray luminosity (and thus higher overall percentage of the total luminosity), but a smaller characteristic radius  $R$  than the broken power-law model.

The average bolometric luminosities (from the profile fit out to 100 arcsec) span the range  $6\text{--}43 \times 10^{44} \text{ erg s}^{-1}$ , with values of 13 and  $18 \times 10^{44} \text{ erg s}^{-1}$  being typical for the broken power-law and

**Table 3.** Average properties of the extended component.

| Quasar<br>outer radius (arcsec) | $R$ (kpc)<br>(50) | %<br>(50)  | $L_{\text{bol}}$ ( $10^{43}$ erg $\text{s}^{-1}$ )<br>(50) | $R$ (kpc)<br>(100) | %<br>(100) | $L_{\text{bol}}$ ( $10^{43}$ erg $\text{s}^{-1}$ )<br>(100) |
|---------------------------------|-------------------|------------|--|--------------------|------------|---|
| 3C48 (King)                     | $33 \pm 4$        | $13 \pm 1$ | $154 \pm 13$   | $35 \pm 2$         | $15 \pm 2$ | $180 \pm 20$  |
| " (BPL)                         | $39 \pm 1$        | $11 \pm 1$ | $119 \pm 7$  | $39 \pm 1$         | $11 \pm 1$ | $128 \pm 9$   |
| 3C215 (King)                    | $32 \pm 1$        | $26 \pm 3$ | $85 \pm 11$  | $33 \pm 1$         | $26 \pm 4$ | $89 \pm 13$   |
| " (BPL)                         | $49 \pm 3$        | $17 \pm 3$ | $57 \pm 9$   | $49 \pm 3$         | $19 \pm 3$ | $68 \pm 11$   |
| 3C254                           | $86 \pm 10$       | $16 \pm 2$ | $121 \pm 9$  | $94 \pm 11$        | $17 \pm 1$ | $141 \pm 4$   |
| 3C273 (King)                    | $15 \pm 1$        | $10 \pm 1$ | $353 \pm 22$   | $14 \pm 1$         | $12 \pm 1$ | $426 \pm 17$  |
| " (BPL)                         | $31 \pm 2$        | $5 \pm 1$  | $173 \pm 2$  | $31 \pm 2$         | $5 \pm 1$  | $166 \pm 2$   |
| 3C275.1                         | (341)             | (17)       | (40)   | $270 \pm 7$        | $24 \pm 1$ | $62 \pm 4$  |
| 3C281 (King)                    | $39 \pm 1$        | $62 \pm 6$ | $256 \pm 3$  | $38 \pm 1$         | $64 \pm 4$ | $276 \pm 3$   |
| " (BPL)                         | $50 \pm 2$        | $45 \pm 3$ | $189 \pm 8$  | $48 \pm 5$         | $47 \pm 4$ | $213 \pm 2$   |
| 3C334                           | $50 \pm 10$       | $16 \pm 3$ | $106 \pm 18$   | $49 \pm 9$         | $17 \pm 3$ | $117 \pm 18$  |
| H1821 + 643 (King)              | $175 \pm 12$      | $11 \pm 1$ | $218 \pm 11$   | $267 \pm 18$       | $18 \pm 1$ | $380 \pm 9$   |
| " (BPL)                         | $196 \pm 6$       | $13 \pm 1$ | $254 \pm 11$   | $389 \pm 56$       | $20 \pm 1$ | $431 \pm 11$  |

Notes:

These values are averaged only from the results to the fits to the wobble-corrected images (and each phase interval employed), and from the PSF + broken power-law and PSF + King law models. Where the two models give consistently different answers, we deduce an average for each (e.g. 3C48); where there is a similar range or too few fits available to discriminate reliably for such differences (e.g. 3C275.1) we obtain an average value from both models together.

The errors given are the variation in this average value and not a significance of the detection.

King models respectively. The King models give values of  $R$  in the range 33–38 kpc, with the exception of 14 kpc for the fits to 3C273; for the broken power-law model the values are 31–49 kpc. The three quasars, 3C334, 3C254 and 3C275.1, for which we do not differentiate between parameters derived from each model, have an average  $R$  of 49, 94 and 270 kpc, respectively.

Where a preference between the two models for the extended emission can be seen, it is nearly always for the King law over the broken power-law model (in 3C48, 3C273, 3C281 and 3C334). An exception is the 100-arcsec profile of 1821+643, which is better matched by the broken power-law fits. The continuing increase in luminosity of the extended X-ray emission between the 50- and 100-arcsec profile fits also shows that this component is truly extends over cluster-wide scales of  $\sim 400$ – $800$  kpc radius.

We note that the discrepancy between the observed, corrected profile and the PSF is smallest for 3C273 and 3C48, which are the nearest 3CR quasars in our sample. If there are systematic errors associated with the wobble correction that we are unaware of, then these objects will be the most seriously affected. It is important that the extended emission from these objects be confirmed with *Chandra*.

## 5 DISCUSSION

We plot the average bolometric luminosity of the extended cluster component (from Table 3) against quasar redshift in Fig. 3. For comparison we plot the bolometric luminosity of the X-ray source associated with the distant radio galaxies 3C277.2, 3C294, 3C324, 3C356, 3C368 (from Crawford & Fabian 1996b) and 1138-262 (Carilli et al. 1998), and the clusters surrounding the two nearby FR II radio galaxies Cygnus A (Ueno et al. 1994) and 3C295 (Henry & Henriksen 1986). The observed count rates of the distant radio galaxies have been converted to luminosities assuming the same 4-keV thermal bremsstrahlung model used to obtain luminosities for the quasar extended emission.

The luminosities we have derived for the environment of our quasars are brighter than the upper limits of  $1.6$ – $3.5 \times 10^{44}$  erg  $\text{s}^{-1}$  (rest-frame 0.1–2.4 keV) to any cluster emission surrounding the three radio-loud quasars in Hall et al. (1995; 1997). We note,

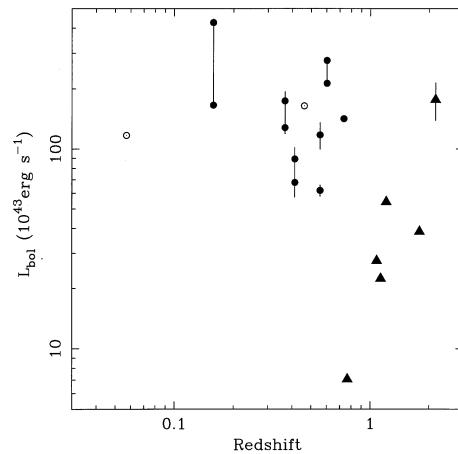


**Figure 3.** The average bolometric luminosities (as given in Table 3) for the extended component of emission (solid circle markers; values extracted from the 100-arcsec profile fits) plotted against the redshift of the quasar. Separate averages obtained for the same quasar assuming the King or broken power-law models are plotted as two points at the same redshift joined by a straight line (where the King law gives the upper end of the range). The luminosities of the host clusters of the nearby FR II radio galaxies Cygnus A and 3C295 are plotted as open circles. The luminosities of the X-ray sources associated with the distant radio galaxies 3C277.2, 3C294, 3C324, 3C356, 3C368 and 1138-262 are also plotted (triangle markers), where the observed count rates have been converted to X-ray luminosities assuming the same 4-keV thermal bremsstrahlung model used for the quasar extended emission.

however, that those upper limits have been obtained from images *not* corrected for satellite wobble. They also assume therefore that the quasar light follows the standard HRI PSF derived by David et al. (1995) and accounts for all the light in the innermost bin. Our quasar host clusters are consistent with the luminosity of  $3.7 \times 10^{45}$  erg  $\text{s}^{-1}$  detected by Hall et al. (1997) for the environment of the radio-intermediate quasar H1821+643 at a redshift  $z = 0.297$ .

The inferred bolometric luminosities of the extended components we have found here are completely reasonable for

**Table 4.** Derived cooling-flow parameters.

| Quasar  | $L_{CF}$<br>( $10^{43}$ erg s $^{-1}$ ) | $\dot{M}$<br>( $M_{\odot}$ yr $^{-1}$ ) | $r_{CF}$<br>(kpc) | $P(30$ kpc)<br>( $10^6$ cm $^{-3}$ K) | $n(R)$<br>( $10^{-2}$ cm $^{-3}$ ) |
|---------|---|---|-------------------|---------------------------------------|------------------------------------|
| 3C48    | 36                                      | 330                                     | 155               | 3.5                                   | 3.4                                |
| 3C215   | 18                                      | 160                                     | 120               | 2.2                                   | 1.7                                |
| 3C254   | 45                                      | 410                                     | 165               | 2.7                                   | 1.2                                |
| 3C273   | 59                                      | 510                                     | 175               | 5.1                                   | 6.2                                |
| 3C275.1 | 30                                      | 100                                     | 110               | 1.4                                   | 0.2                                |
| 3C281   | 58                                      | 510                                     | 180               | 4.0                                   | 3.0                                |
| 3C334   | 33                                      | 290                                     | 150               | 3.1                                   | 2.3                                |

Notes:

$L_{CF}$  is the X-ray luminosity of the extended component within the break radius  $R$ , and is assumed to be caused by a cooling flow in the cluster.

$\dot{M}$  is the derived mass cooling rate within radius  $R$ .

$P$  is the gas pressure at a radius of 30 kpc from the centre of the cluster.

$n(R)$  is the electron density at radius  $R$ .

moderately rich clusters of galaxies at low redshift. They are comparable to the luminosities of the clusters associated with the powerful radio galaxies Cygnus A and 3C295. They are however (Fig. 3) more luminous than the extended X-ray emission detected around more distant 3CR radio galaxies above a redshift of 1. Whether this indicates evolution, a problem for radio galaxy/quasar unification, or is a result of small number statistics must await the compilation of a complete sample, which our study is not.

All extended models have a central cooling time considerably shorter than a Hubble time. We therefore explore the properties of the implied cooling flows occurring around these quasars by deriving some approximate parameters from the broken power-law fits to the profiles. We attribute all the X-ray luminosity of the extended component within radius  $R$  to thermal bremsstrahlung from a gas with electron density  $n$  (where  $n \propto r^{-1}$ ) at a temperature of 4 keV. The cooling time of the gas at  $R$  (except in the case of 3C275.1) is then between about 1 and 3 billion yr. We then estimate the cooling-flow radius  $r_{CF}$  at which the cooling time is  $10^{10}$  yr and obtain a rough indication of the mass deposition rate within that radius from the ratio of the mass of gas within  $r_{CF}$  to  $10^{10}$  yr. The derived values are shown in Table 4. Note that they are of course subject not only to the appropriateness of the fixed slopes chosen for our original broken power-law model, but also to the true gravitational potential of any cluster, and the amount of gravitational work done on the cooling gas. The values should be regarded as uncertain by at least a factor of 2. They may be underestimated by a factor of at least 2 if the gas temperatures are significantly higher than the 4 keV assumed and there is internal absorption, such as is common in low-redshift cooling flows.

Note that the radius of the surface brightness break that we infer is in the range 40–90 kpc, and is similar to the break radius in the profile of the cluster around IRAS 09104 ( $\sim 60$  kpc, Crawford & Fabian 1995b). This is likely to be the radius of the core of the gravitational potential of the cluster; the  $r^{-1}$  profile then occurs within this radius because the gas is cooling at approximately constant pressure. Such small gravitational core radii are characteristic of relaxed lensing cluster cores such as are associated with massive cooling flows (Allen 1998). The large break radii found for 3C275.1 and H1821+643 do not agree with this picture and require more detailed images.

We can also use our cooling-flow parameters to derive a gas pressure  $P$  at a radius of 30 kpc (see Table 4) for comparison with

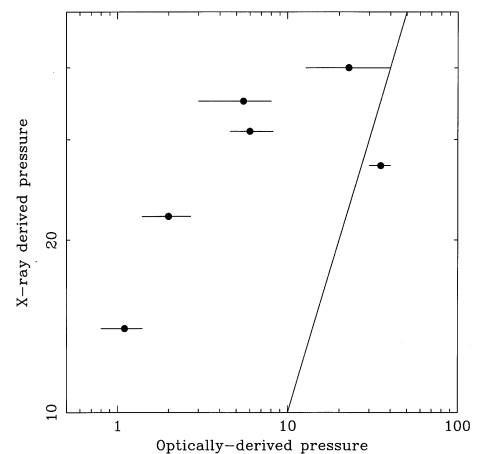


**Figure 4.** Comparison of the gas pressure at a projected distance of 30 kpc from the quasar derived from the ionization state of the extended emission-line gas, and from the broken power-law fits to the X-ray radial profiles. Pressures are expressed in units of  $10^5$  cm $^{-3}$  K, and the solid line indicates the locus of equal pressures.

the pressures derived from the completely independent method using the ionization state of the extended optical emission lines (Crawford & Fabian 1989; Bremer et al. 1992; Crawford & Vanderriest 1997). The pressures derived from the optical nebulosities mostly underestimate those derived from the X-ray profile fits (Fig. 4) by a factor of up to 10. Given that the gas pressures are mostly derived from the optical nebulosity using a conservative underestimate to the crucial but unknown UV and soft X-ray band of the ionizing nuclear spectrum, this discrepancy is not surprising. Support for this interpretation of the disparity in derived pressures is found in Crawford et al. (1991), where a better knowledge of the ionizing continuum of the nucleus of 3C263 was found to increase the optically derived pressure by up to an order of magnitude. In addition, we note that 3C254, the quasar with the best agreement between the two pressure values, is the only one for which UV *HST* data has been used to constrain the shape of the ionizing continuum (Crawford & Vanderriest 1997).

We note that the derived cluster luminosity for 3C273 is high and implies the presence of a rich cluster that is not seen at other wavelengths. At its relatively low redshift of  $z = 0.16$ , such a cluster should be obvious in the optical band. As mentioned already, it has

the profile most susceptible to systematic errors, and the absence of an optical cluster may argue for the existence of such errors. If the PSF is uncertain by a relative amount equal to the difference between observed 3C273 profile and our empirical PSF, then it will not change greatly our results for the other quasars, except perhaps for 3C48.

Inverse Compton scattering of quasar radiation could still contribute to our extended component of X-ray emission. If it were a significant process, the X-ray source would appear asymmetric and lopsided, as (back-)scattering by the electrons should be stronger in the more distant radio lobe than in the nearer lobe (Brunetti et al. 1997). The quality of our current data is insufficient to show any significant asymmetry, and so we are unable to assess the contribution from this process. Observations of these sources with *Chandra* and *XMM* should clarify its relative importance to the total emission.

## 6 CONCLUSIONS

The seven powerful radio-loud quasars studied here appear to be surrounded by luminous extended X-ray emission. The spatial properties of the emission are consistent with an origin in thermal emission from an intracluster medium. The radiative cooling time of the gas within  $\sim 50$  kpc of the quasars is only a few billion years or less, indicating the presence of strong cooling flows of hundreds of  $M_{\odot} \text{yr}^{-1}$ . The high pressure of that gas is sufficient to support the extended optical nebulosities seen around many of these quasars and may play a role in shaping the properties of the radio sources, such as structure, depolarization and possibly even fuelling and evolution (Fabian & Crawford 1990). Such a role is not clear from a comparison of radio properties with the neighbouring optical galaxy density (Rector, Stocke & Ellingson 1995).

A small number of luminous clusters without central AGN have so far been found beyond redshift 0.5, and the discovery of a cluster at  $z \sim 0.8$  with luminosity  $10^{45} \text{erg s}^{-1}$  (Donahue et al. 1998) provides strong evidence for a low-density universe. We have shown that the study of the environment of powerful radio-loud quasars is a promising way of extending the discovery of similarly luminous clusters both in numbers and to higher redshifts.

## ACKNOWLEDGMENTS

We thank Steve Allen for advice on the profiles of massive cooling flows. CSC and ACF thank the Royal Society for financial support. This work has been supported in part by the DLR (format DARA GmbH) under grant 50 OR 9403 5 (GH and IL). This research has made use of the NASA/IPAC Extragalactic Database (NED) and the Leicester Database and Archive Service (LEDAS).

## REFERENCES

- Allen S. W., 1998, *MNRAS*, 296, 392  
 Barthel P. D., Miley G. K., 1988, *Nat*, 333, 319  
 Best P., Longair M. S., Rottgering H. J. A., 1998, *MNRAS*, 295, 549  
 Bower R., Smail I., 1997, *MNRAS*, 290, 292  
 Bremer M. N., Crawford C. S., Fabian A. C., Johnstone R. M., 1992, *MNRAS*, 254, 614  
 Bremer M. N., 1997, *MNRAS*, 284, 126  
 Brunetti G., Setti G., Comastri A., 1997, *A&A*, 235, 898  
 Carilli C. L., Owen F. N., Harris D. E., 1994, *AJ*, 107, 480  
 Carilli C. L. et al., 1997, *ApJS*, 109, 1  
 Carilli C. L., Harris D. E., Pentericci L., Rottergering J. J. A., Miley G. K., Bremer M. N., 1998, *ApJ*, 494, L143  
 Crawford C. S., Jackson N., Pérez-Fournon I., 1997, in Bremer M., Jackson N., Pérez-Fournon I., *Observational Cosmology with the New Radio Surveys*. Kluwer, Dordrecht, p. 99  
 Crawford C. S., Fabian A. C., 1989, *MNRAS*, 239, 219  
 Crawford C. S., Fabian A. C., 1993, *MNRAS*, 260, L15  
 Crawford C. S., Fabian A. C., 1995a, *MNRAS*, 273, 827  
 Crawford C. S., Fabian A. C., 1995b, *MNRAS*, 274, L63  
 Crawford C. S., Fabian A. C., 1996a, *MNRAS*, 281, L5  
 Crawford C. S., Fabian A. C., 1996b, *MNRAS*, 282, 1483  
 Crawford C. S., Fabian A. C., George I. M., Naylor T., 1991, *MNRAS*, 248, 139  
 Crawford C. S., Vanderriest C., 1997, *MNRAS*, 285, 580  
 David L. P., Harnden F. R., Kearns K. E., Zombeck M. V., 1995, *The ROSAT High Resolution Imager*. US *ROSAT* Science Data Center, Smithsonian Astrophysical Observatory  
 Deltorn J. M., Le Fevre O., Crampton D., Dickinson M., 1997, *ApJ*, 483, L21  
 Dickinson M., 1997, in Tanvir N., Aragon-Salamanca A., Wall J. V., eds, *HST and the High Redshift Universe*. World Scientific, Singapore  
 Donahue M., Voit G. M., Gioia I., Lupino G., Huges J. P., Stocke J. T., 1998, *ApJ*, 502, 550  
 Durret F., Pecontal E., Petitjean P., Bergeron J., 1994, *A&A*, 291, 392  
 Ebeling H., Edge A. C., Fabian A. C., Allen S. W., Crawford C. S., Böhringer H., 1997, *ApJ*, 479, L101  
 Ebeling H. et al., 1998, *MNRAS*, 301, 881  
 Ellingson E., Yee H. K. C., Green R. F., 1991, *ApJS*, 76, 455  
 Fabian A. C., Crawford C. S., 1990, *MNRAS*, 247, 439  
 Fabian A. C., Crawford C. S., Johnstone R. M., Thomas P. A., 1987, *MNRAS*, 228, 963  
 Forbes D. A., Crawford C. S., Fabian A. C., Johnstone R. M., 1990, *MNRAS*, 244, 680  
 Garrington S. T., Conway R. G., 1991, *MNRAS*, 250, 198  
 Garrington S. T., Conway R. G., Leahy J. P., 1991, *MNRAS*, 250, 171  
 Hall P. B., Ellingson E., Green R. F., Yee H. K. C., 1995, *AJ*, 110, 513  
 Hall P. B., Ellingson E., Green R. F., 1997, *AJ*, 113, 1179  
 Hardcastle M. J., Worrall D. M., 1999, *MNRAS*, in press  
 Hardcastle M. J., Lawrence C. R., Worrall D. M., 1998, *ApJ*, 504, 743  
 Harris D. E., Stern C. P., 1987, *ApJ*, 313, 136  
 Harris D. E., Silverman J. D., Hasinger G., Lehmann I., 1998, *A&AS*, 133, 431  
 Henry J. P., Henriksen M. J., 1986, *ApJ*, 301, 689  
 Hes R., 1995, PhD thesis, Univ. Groningen  
 Hill G. J., Lilly S. J., 1991, *ApJ*, 367, 1  
 Hintzen P., 1984, *ApJS*, 55, 533  
 Hintzen P., Romanishin W., 1986, *ApJ*, 311, L1  
 Hintzen P., Stocke J. T., 1986, *ApJ*, 308, 540  
 Hintzen P., Boeshaar G., Scott J., 1981, *ApJ*, 246, L1  
 Hintzen P., Ulvestad J., Owen F. N., 1983, *ApJ*, 88, 709  
 Lehmann I., Hasinger G., Schwöpe A. D., Böller Th., 1999, preprint (astro-ph/9810214)  
 Liu R., Pooley G., 1991, *MNRAS*, 249, 343  
 Morse J. A., 1994, *PASP*, 106, 675  
 Rector T., Stocke J. T., Ellingson E., 1995, *AJ*, 110, 1492  
 Rosati P., Della Ceca R., Norman C., Giacconi R., 1998, *ApJ*, 492, 21  
 Stark A. A., Gammie C. F., Wilson R. W., Bally J., Linke R. A., Heiles C., Hurwitz M., 1992, *ApJS*, 79, 77  
 Stockton A., 1980, in Abell G. O., Peebles P. J. E., eds, *IAU Symp. 92, Objects of high redshift*. Reidel, Dordrecht, p. 89  
 Ueno S., Koyama K., Nishida M., Yamauchi S., Ward M. J., 1994, *ApJ*, 431, L1  
 Worrall D. M., Lawrence C. R., Pearson T. J., Readhead A. C. S., 1994, *ApJ*, 420, L17  
 Yates M. G., Miller L., Peacock J. A., 1989, *MNRAS*, 240, 129  
 Yee H. K. C., Green R. F., 1987, *ApJ*, 319, 28  
 Yee H. K. C., Green R. F., Stockman H. S., 1986, *ApJS*, 62, 681